## NEUTRON NUCLEAR PHYSICS

In 2017, in FLNP the scientific activity in the field of neutron nuclear physics was carried out in the following traditional directions: investigations of time and space parity violation processes in neutron-nuclear interactions; studies of the fission process; experimental and theoretical investigations of fundamental properties of the neutron; gamma-spectroscopy of neutron-nuclear interactions; atomic nuclear structure, obtaining of new data for reactor applications and nuclear astrophysics; experiments with ultracold neutrons, applied research using NAA. The scientific program to study the inelastic scattering of fast neutrons ("TANGRA" project) is being successfully implemented. Despite some technical difficulties, the second stage of the LUE-200 accelerator was commissioned, and a series of applied studies were conducted on neutron beams of the IREN facility. A number of investigations in the field of fundamental physics and ultracold neutron physics were performed on the neutron beams of nuclear research centers in Germany, China, USA, France, Switzerland.

### Measurement of ROT effect for gamma-rays in $^{235}$U fission on a hot source of polarized neutrons

In the framework of the FLNP JINR – ITEP – FRM-II collaboration a series of experiments was continued to measure the ROT-effect in the emission of prompt γ-rays and neutrons in binary fission of $^{235}$U and $^{233}$U induced by polarized cold neutrons. The experiments were carried out on the POLI instrument at the FRM-2 reactor (Garching, Germany).

T-odd effects in the fission of heavy nuclei have been known for more than ten years. The first effect of this type (the so-called TRI-effect) was detected at the ILL reactor (Grenoble) by the collaboration of Russian and European institutes in the experiment aimed at finding a violation of the time reversal invariance (TRI) following the idea proposed by K. Schreckenbach. It was found that the probability of emission of an alpha particle in a ternary fission in the direction perpendicular to the plane formed by the neutron spin and the fragment momentum demonstrates a pronounced anisotropy. The magnitude of the effect turned out to be surprisingly high, and the current explanation does not imply the existence of such a violation, but is based on the interaction of the reaction products in the final state. In other words, the effect is not related to the violation of the invariance with respect to time reversal, but is connected with the mechanism of the fission process. Nevertheless, in the literature the effect is still called "TRI-effect".

In addition, it was noted that when the direction of the neutron beam polarization is changed, the angular distribution of α-particles is shifted by a small angle relative to the fragment emission axis, and the direction of the shift is determined by the direction of the neutron beam polarization. The authors called this effect ROT-effect. Both TRI- and ROT-effects are formally T-odd, but have no direct connection with the violation of time reversal invariance.

From the quasi-classical description of the ROT effect, which assumes the rotation of a polarized nucleus before its splitting into two (or three) fragments, it follows that an analogous phenomenon can be observed in the angular distribution of some other particles accompanying the fission of the nucleus into two fragments, if this distribution is anisotropic with respect to the axis of the deformation of the fissioning nucleus at the time of splitting, and the asymmetry relative to the initial direction of the deformation axis is completely or partially preserved after the fragments escape to infinity. Indeed, the analogous effect was observed in the emission of instant gamma-

rays and neutrons in the fission of $^{235}$U and $^{233}$U, though its magnitude was an order of magnitude smaller than for the emission of *α*-particles in triple fission.

At present, there are several theoretical models that can describe both effects. According to the model proposed in 2016, both effects depend on the quantum numbers J and K which characterize the fission channels. In fission induced by thermal (or cold) neutrons (for which all previous data were obtained), there is a mixture of several spin states whose contributions are unknown. The only way to obtain "clean" data is to perform measurements on isolated resonances. Such an experiment was carried out on the POLI facility at the FRM-II reactor in Garching, which provides a required polarized neutron beam of hot neutrons with an energy of 0.27 eV corresponding to the lowest resonance of $^{235}$U.

A schematic of the experimental setup is shown in **Fig. I-3-1**. A narrow neutron beam was monochromatized by a monochromator made of a mosaic of Cu crystals to the average energy of 270 meV (λ = 0.55 Å). The monochromator also makes it possible to simultaneously focus the neutron beam at a given position, providing maximum intensity of unpolarized neutrons of about $4 \cdot 10^6$ n/cm$^2$/s.

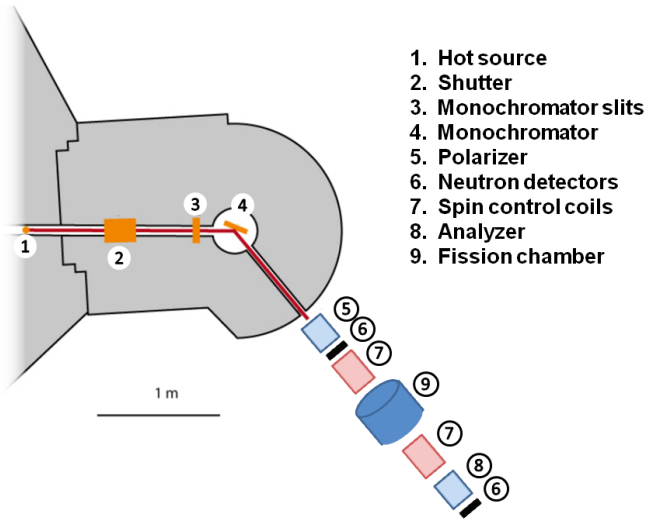


***Fig. I-3-1.*** *Schematic of the experimental setup at the POLI facility of the FRM-II reactor.*

Neutrons were polarized using specially constructed $^3$He cells. The same cell type was used as an analyzer for measuring beam polarization. Since polarized $^3$He nuclei have a very high spin-dependent neutron absorption efficiency over a wide energy range, a $^3$He cell can be used as a broadband neutron polarizer or analyzer with the possibility of optimizing its efficiency for almost all neutron wavelengths. In our experiment, the cell size of Ø60 x 130 mm and a pressure of 2.5 bar ensured maximum neutron polarization of about 70%. The polarizer and analyzer cells were polarized in an external laboratory and placed in a special magnetic housing with a strong uniform constant magnetic field. Polarization of $^3$He in the cell decreased exponentially with a time constant of about 40 h, so both cells were replaced every 24 h.

Both the polarizer and analyzer provided vertical neutron beam polarization, while the effect under study requires horizontal (longitudinal) polarization. To change the polarization direction from vertical to horizontal, a specially developed spin control system consisting of several magnetic coils with a μ-metal screen was used, which also made it possible to rotate the spin in a given position by 180$^o$ every 1.3 s.

A schematic of the fission chamber surrounded by a set of gamma-ray detectors is shown in **Fig. I-3-2**. The chamber is filled with $CF_4$ gas at a pressure of about 10 mbar. The uranium target containing about 82 mg of $^{235}U$ (99.99%) oxide deposited on both sides of a thick aluminum substrate with a thickness of 40 × 100 $mm^2$ was positioned on the chamber axis. Thin low-pressure multiwire proportional counters (MWPC) placed on both sides of the target were used as detectors for fission fragments. Eight cylindrical plastic scintillators and four NaI-based scintillators were inserted into the rotating holder at a distance of about 30 cm from the target center, which provided subsequent measurements of the coincidences of instant gamma-rays and neutrons with fission fragments at the angles of ± 22.5, ± 45, ± 67.5, ± 112.5, ± 135 and ± 157.5° relative to the average fragment detection axis. The detectors of gamma-rays and fission fragments were located in the plane orthogonal to the neutron beam direction, which also coincides with the polarization axis of $^{236}U$ nuclei.

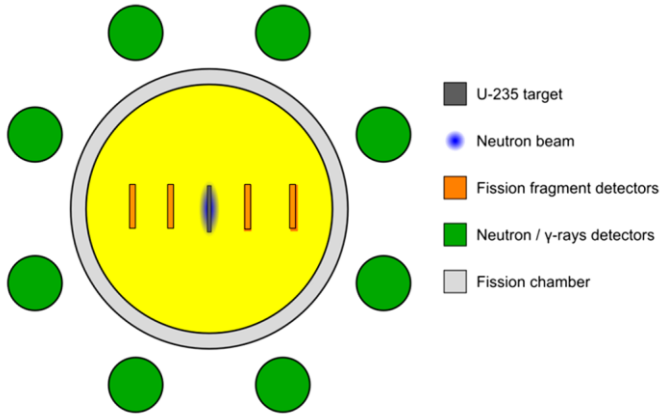


*Fig. I-3-2. Schematic of the fission chamber.*

Separation of instant neutrons and γ rays could be done using the time-of-flight technique (**Fig. I-3-3**). Each event matching coincidence of signals from neutron and fragment detectors is digitized by multichannel TDC CAEN V775N and stored together with the information about the direction of polarization of the neutron beam. Reverse of polarization occurs at a frequency of 1 Hz; the input signal of TDC is delayed by the spin flip time of the neutron. At the same time, for the on-line control of the setup, the coincidence count rates of neutrons/γ-rays and fission fragments were registered by counters which were read out every 5 min for each detector. The values of asymmetries, calculated by the formula $R=(N^+ - N^-)/(N^+ + N^-)$ were constantly monitored. Here $N^+$ and $N^-$ are the coincidence count rates for opposite directions of neutron polarization. The asymmetry of count rates of the fragments was simultaneously measured and controlled.

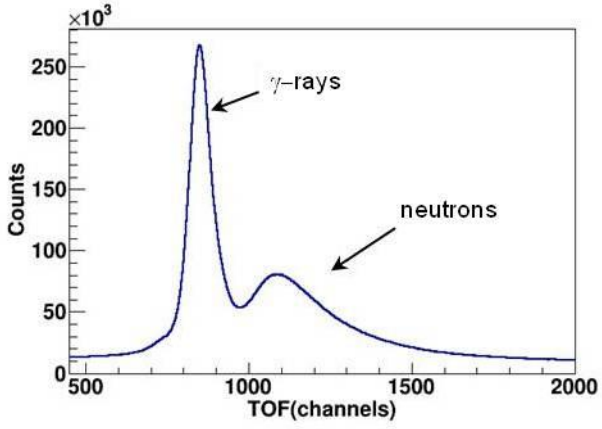


*Fig. I-3-3. Time-of-flight spectrum from a plastic detector allowing separation of gamma-rays and neutrons.*

The total time for the experiment at the POLY facility was 27 days. The installation, detector calibration, adjusting of the spin control system, and so on took five days. Statistics was accumulated during 22 days.

Also, the measurment of neutron fluxes in the experiment gave $2 \cdot 10^7$ $cm^{-2}$ $s^{-1}$ at the exit from the neutron channel (i.e. at the entrance of the polarizer) and $3.3 \cdot 10^7$ $cm^{-2}$ $s^{-1}$ at the front part of the fission chamber.

A full analysis of the experimental data will take quite a long time. The only conclusion that can be drawn at this stage of analysis is that the statistical uncertainty of the experimental data is about half of that obtained in 2016. At the same time, the sensitivity of the new experimental setup is approximately 5 times higher, mainly due to the use of position-sensitive detectors of fission fragments. Such statistical accuracy and sensitivity would certainly be sufficient to observe the effect, if its magnitude were the same as the measured effect in the region of cold neutrons. However, a new model of the ROT-effect (proposed recently) predicts a decrease of the effect in the 0.3 eV resonance of $^{235}U$. The preliminary analysis of the data shows that the effect actually diminishes, but a more detailed analysis is required to obtain its exact value or determine its upper limit.

**Investigation of prompt neutron emission in neutron induced nuclear fission**

In 2016-2017 a complex spectrometer consisting of a double ionization chamber with Frisch grids (DIC) and a scintillation (BC501) fast neutron detector was developed and designed in the Department of Nuclear Physics. The spectrometer is intended for experimental studies of fission processes in the late stages of the evolution of the fissioning system (after passing through the "saddle point") using the IBR- and IREN neutron sources. To date, fission in the reactions $^{252}Cf(sf)$, $^{235}U(n_{res},f)$, $^{235}U(n_{th},f)$, have been studied; for which masses of correlated fission fragments (FF), their kinetic energies and the cosines of the angles ($\Theta_{1,2}$) between the direction of FF emission and the fixed axis of a cylindrical coordinate system, were measured. Since the detector was located at a fixed distance from the coordinate system, the measured cosines of the angles ($\Theta_{1,2}$) were equal to the cosines of the angles between the direction of FF emission and prompt fission neutrons (PFN) emitted in the fission process. The fast neutron detector made it possible to measure the speed of PFN and suppress the background of prompt gamma-radiation by analyzing the pulse shape.

The implementation of the procedure for determining these characteristics for each fission event became possible due to the use of synchronous ADCs that simultaneously sampled detector pulses at a frequency of 250 MHz and amplitude resolution of 12 bits. The launching of these digitizers was done with the help of specially developed electronic equipment in the NIM standard, hereinafter referred to as the "trigger". The unit could generate pulses to trigger the sampling of detector pulses and store them in the local ADC memory. The ADCs had a local segmented high-capacity memory that made it possible to organize data acqusition in the local ADC memory practically without dead time (since the data from the local ADC memory were transferred to the PC memory in the intervals between the source pulses). The pulse digitizer was installed in the PCIe bus expansion module of the PC motherboard. The communication of the specified module with PC was carried out through the optical interface "SONET". Specially developed PC software

could specify synchronization modes, acqusition algorithms, storage in the local memory and transformation of obtained data to PC for on-line or off-line processing modes, as well as data storage. At present, two sets of spectrometer electronics have been manufactured, one of which is used at IBR-2 and the other at IREN. The experimental study of the PFN emission process in the $^{235}U(n_{th},f)$ reaction was necessary, since the available data were obtained more than 50 years ago and are somewhat ambiguous. New measurements were made on IBR-2 beamline 11B equipped with a curved mirror neutron guide effectively suppressing gamma radiation from the neutron source. The obtained results [1] made it possible to correct the available data and for the first time obtain FF mass distribution, which is in good agreement with the data obtained at a spectrometer with a resolution of about 0.5 amu. The dependence of the number of PFN on FF mass carries very important information on the impact of quantum effects (nuclear shells of forming FF) on the FF formation processes. For example, in **Fig. I-3-4**, the experimental data acquired under identical conditions with identical detectors obtained in the reactions $^{252}Cf(sf)$ and $^{235}U(n_{th},f)$ are given for comparison.

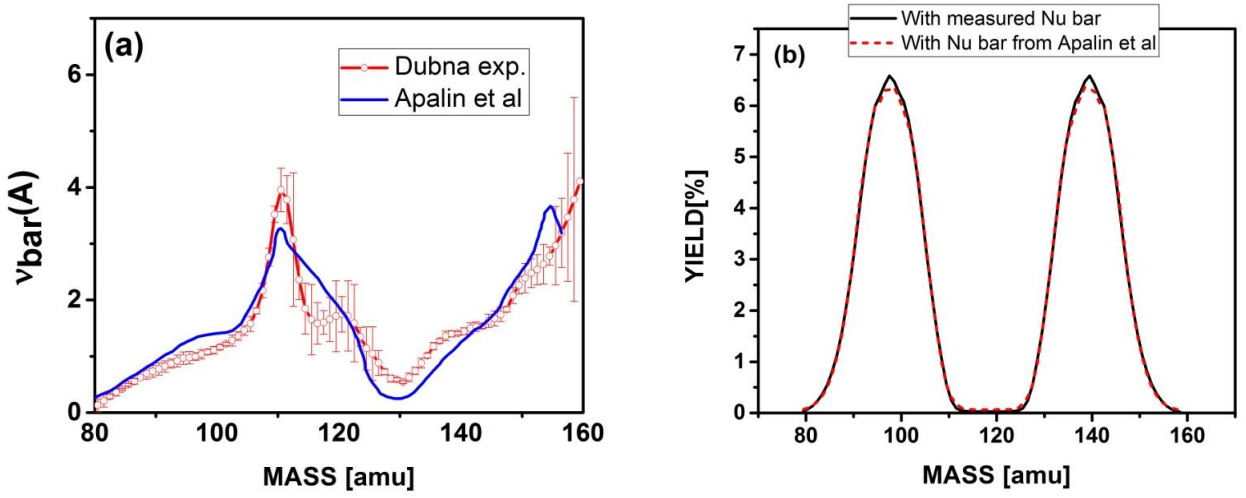


*a)* *b)*

***Fig. I-3-4.*** *a) Comparison of dependence of PFN average number in $^{235}U(n_{th},f)$ reaction obtained in Dubna with the results published in [2]. b) Comparison of mass distributions obtained using our data and data from [3].*

The PFN yield for fragments with mass numbers in the region of A ~ 118 for the $^{235}U(n_{th},f)$ reaction is siginificantly lower than for the $^{252}Cf(sf)$ reaction (**Fig. I-3-5**). This is a consequence of the fact that the shell of the correlated fragment for $^{252}Cf$ is almost filled whereas for $^{235}U$ in the region of A ~ 120 the shells of both fragments are half-filled. Nuclei with filled shells have a shape close to a spherical one and, hence, a more tightly bound structure that resists deformation more strongly. Another argument in favor of greater incompactness of nuclei with unfilled shells is the fact that in the $^{252}Cf(sf)$ reaction the average PFN number is larger than in the $^{235}U(n_{th},f)$ reaction due to a higher PFN yield in the region of A ~ 120 for $^{252}Cf(sf)$. The anomalously small PFN yield in the region of A ~ 132 is explained by high stability of the spherical configuration in this region and high resistance of the correlated fragment to deformation (high rigidity of configuration [4]). As the

excitation energy increases, the shell effects are suppressed and configurations of fissioning nuclei become more elongated with a lower total kinetic energy (TKE) and an increase in the total deformation energy (TDE) of the fragments. In this case, mainly the excitation energy of heavy fragments increases. This phenomenon was usually explained by the fact that during the formation of fragments, an intensive energy exchange occurs between the fragments with a uniform energy distribution between the degrees of freedom. Since a heavy fragment has a greater number of degrees of freedom, it takes a larger portion of the excitation energy.

From this it was also concluded that the excitation energy is spent to increase the temperature of the fragments at equal temperatures of the fragments. However, the experiments studying the nuclear level density in the energy range of up to 6-7 MeV show that the last statement is incorrect. The temperature of nuclei does not change with increasing excitation energy due to the fact that pair correlations lead to an effective increase in the number of degrees of freedom in the nuclei in proportion to the increase in their excitation energy [5]. Cooper pairs of neutrons and protons decay so that the average excitation energy per nucleon, and, hence, the temperature, remains constant. However, due to the differences in the level densities, the temperature of the light FF appears to be higher than the temperature of the heavy FF. The fissioning nucleus up until the point of rupture can be considered as two independent nuclei connected by a neck and being in thermal contact [6]. The superfluidity mode leads to the fact that the energy transfer between FFs occurs during the transition of Cooper pairs from the light to heavy FF, in which pairs have a lower binding energy and decay with higher probability. Since the number of degrees of freedom increases after pair decay, the temperature of the heavy FF does not change, but its excitation energy increases. This effect, as proposed by the authors of [6], explains the reason for the increase in the number of PFN (mainly through the increase in the excitation energy). However, if a heavy FF has a shape close to a spherical one (closed outer shell) then the energy transfer process can go in reverse. Thus, the study of the PFN emission process in fission is of special interest, especially regarding the dependence of the average number of PFN on the fragment mass, since the variations in the number of PFN are directly related to the process of excitation energy redistribution between the fragments.

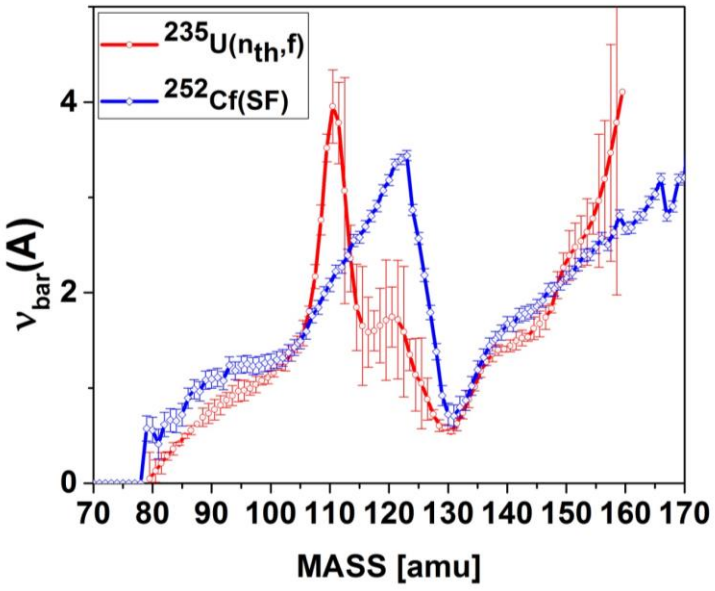


*Fig. I-3-5. Comparison of the average number of PFN in the $^{235}U(n_{th},f)$ reaction with the results for $^{252}Cf(sf)$.*

**Position-sensitive ionization chamber for the investigation of PFN in resonance neutron induced fission**

The progress in understanding the fission process is largely due to the development of more advanced experimental methods. The rapid development of electronics and information technology has recently been one of the most powerful incentives for increasing the informativeness of experimental research. A huge role in this was played by the development of digital technologies, which by now have almost completely superseded the traditional analog paradigm not only in nuclear physics, but also in the modern industry. A significant improvement in the systems of detector signal normalization became possible due to the miniaturization of electronics, which allowed the creation of compact equipment for position-sensitive detectors. Owing to these technical achievements, we succeeded in designing a compact position-sensitive double ionization chamber (DIC) for FF spectrometry. The developed design of DIC [7-9] allowed simultaneous measurement of kinetic energies, masses and orientation of FFs in a 3D cylindrical coordinate system. As noted above, the most valuable information on the fission process can be obtained in PFN emission studies. The application of the DIC developed in the work makes it possible to increase the efficiency of these experiments by more than an order of magnitude due to the use of a larger number of fast neutron detectors. The development of the detector was carried out in two stages. At first, specialized software was created to calculate 2D electrostatic fields, necessary for studying charge induction on the chamber electrodes during the drift of electrons in ionization chambers. As a result, the ambiguities in the procedures for determining the amplitudes and directions of the FF motion were eliminated. Then, the programs were improved in order to be used for studying charge induction on the electrodes of the position-sensitive DIC with strip anodes. Numerical simulation was carried out for two variants of signal processing organization, and both variants were realized and tested. At present, data have been processed only for one of the variants. As a result of numerical simulation, it was found that the magnitude of the induced charges in the chain of anode strips in the cross-section Y = const is proportional to the ratio of the lengths of the strip segments along the Y axis. It was assumed that the projection of the particle trajectory along the Y axis is directed along the Y axis. The scheme of arrangement of electrodes in the chamber is presented in **Fig.I-3-6**.

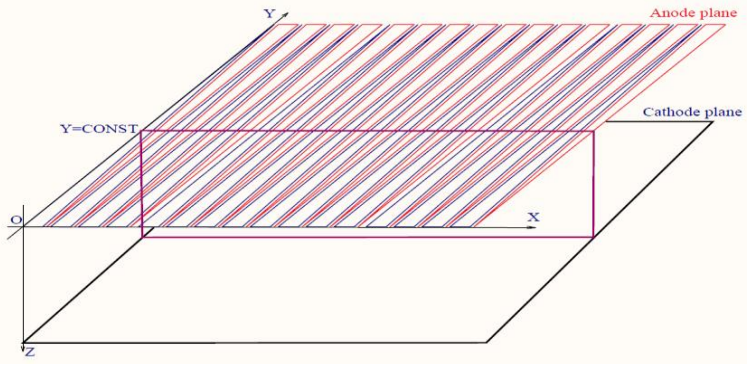


***Fig. I-3-6.*** *Design of ionization chamber with strip anodes. Pair of strips (red and blue) is formed by cutting a rectangular metal plate along diagonal.*

**Figure I-3-7** shows the dependence of the calculated weighting potential in the plane Y = const for one strip under unit potential and zero potential on all other electrodes in the chamber. According to the Shockley-Ramo theorem, the charge induced in the chains of adjacent strips when electrons moving in the plane Y = const from point *a* to point *b* can be calculated by

formula (1), where Q is the induced charge, *e* is the electron charge, $\Phi(a)$ and $\Phi(b)$ are weighting potentials at points *a* and *b*, respectively.

$$Q = e \cdot (\Phi(a) - \Phi(b)) \quad (1)$$

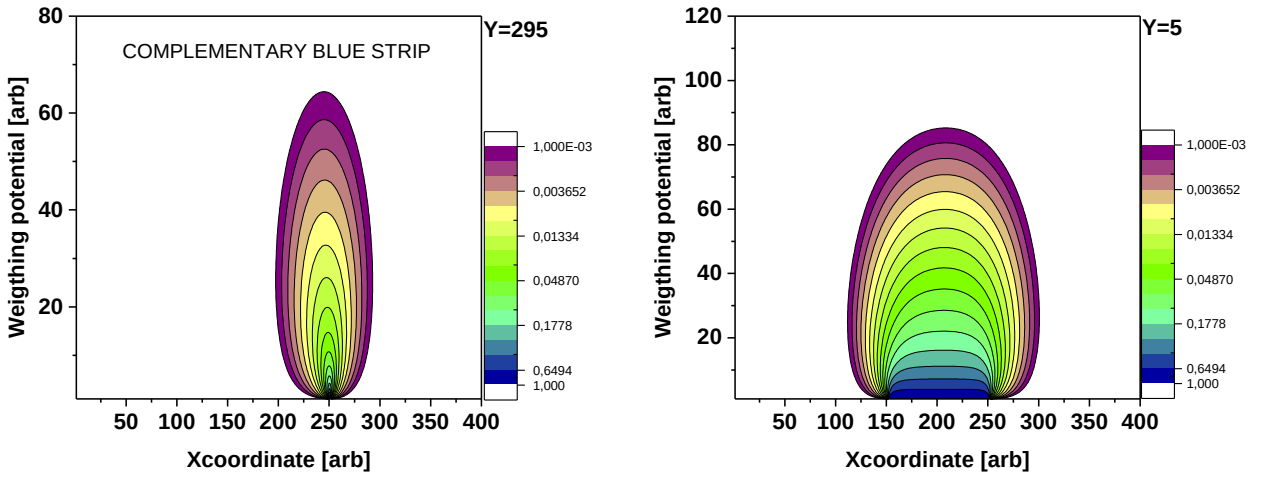


***Fig. I-3-7.*** *Coordinate dependence of charge induced in chain filter.*

From the analysis of the graphs in **Fig. I-3-7** it follows that under the conditions indicated above the ratio of the charge induced on the strip is proportional to the Y coordinate with a uniform ionization density in the plane Y = const. To verify the results of the calculations, measurements were made with the chamber shown schematically in **Fig. I-3-6**. To encode coordinates, an electronic strip connection circuit was proposed (**Fig. I-3-8**).

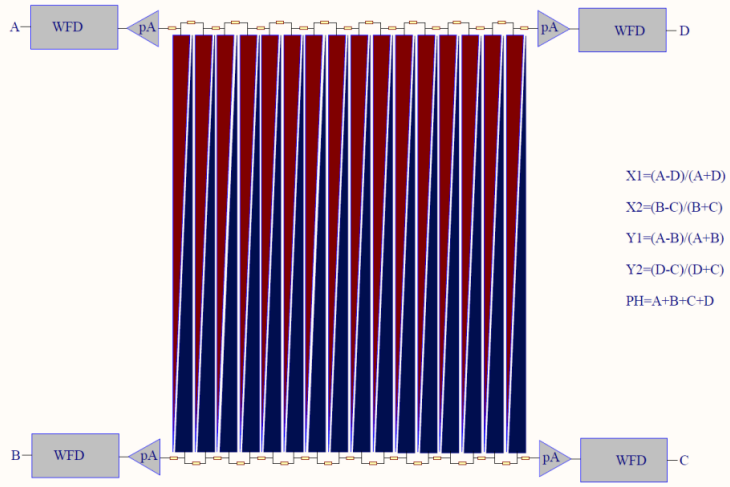


***Fig. I-3-8.*** *Scheme of strip connection to resistive chain filter. Blue and red strips are electrically isolated from each other.*

With this type of connection, the electrical capacitance of the strips together with the resistors connecting the adjacent strips formed two chain filters. The charge induction on the strip was transformed into current pulses in both chains of the chain filters. The pulse propagation in the chain filters was investigated using the operational calculus. The links of the chain filters were considered as passive four-poles with a wave impedance load at the ends. In this case, the current pulse is transmitted without distortion, and it was shown that the induced charge

is divided equally between the strips and propagates towards the corresponding ends of the chain filters. The fact that the pulse propagation causes a decrease in the pulse amplitude proportional to the number of the filter links was used to determine the point of the charge injection into the chain filter. As was shown above, the charges induced in adjacent strips are divided proportionally to the distance between the injection point and the middle of the strips:

$$y = L_y \cdot \left(\frac{1}{2} + \frac{Q_A - Q_B}{Q_A + Q_B}\right) \quad (2),$$

$$x = L_x \cdot \left(\frac{1}{2} + \frac{Q_A - Q_D}{Q_A + Q_D}\right) \quad (3).$$

Thus, formula (2) gives the y-coordinate of the "center of gravity" of the charge distribution of ionization electrons which arise as a result of deceleration of charged particles in the working volume of the chamber. Similarly, the x-coordinate of the "center of gravity" can be determined using formula (3), where $Q_A$, $Q_B$, $Q_C$ $Q_D$ are the amplitudes of pulses at the terminal points of the chain filters.

To determine the degree of decrease of the pulse amplitude during the pulse propagation in the chain filter, calculations were made for the signal attenuation function after passing K links (in K-range from 0 to 16) of the chain filter. The results are shown in **Fig. I-3-9**.

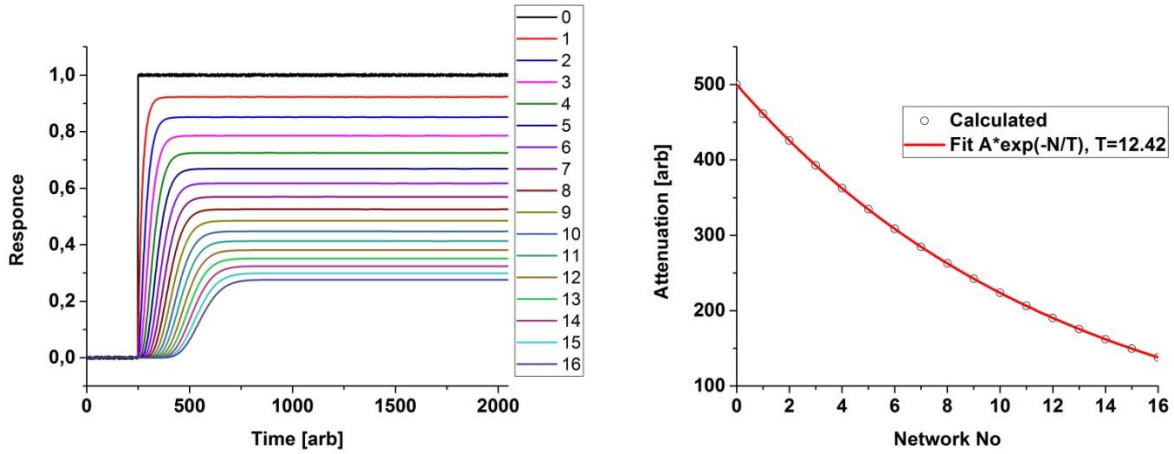


***Fig. I-3-9.*** *Calculations of signal attenuation after passing K links of chain filter.*

These results were used to correct the information on coordinates determined by formulas (2) and (3).

**Empirical model of cascade gamma-decay and studies of parameters that determine superfluid properties of the nucleus**

In 2017, the analysis of the nuclear data obtained with the help of the developed in Dubna empirical model of the cascade gamma decay of the neutron resonance was improved. This model makes it possible (from the approximation of experimental intensities of two-quantum cascades) to determine simultaneously (with percentage accuracy) the parameters of the density of nuclear levels, ρ, and parameters of partial widths, Γ, of the emission of nuclear reaction products. To date, the cascades of two successively emitted gamma-rays have been measured in the capture of thermal neutrons by 44 nuclei in the mass range of 28 < A < 200.

The most probable ρ- and Γ-values can be obtained only from the approximation of intensities of cascades between fixed initial levels and any intermediate and final levels of the excited nucleus. The two-quantum cascade (TQC) is determined by the energies of initial, intermediate and final levels, as well as the probabilities of electromagnetic transitions between them.

After the sequence order of quanta in cascades is determined (using the maximum likelihood method, from the condition that the primary transitions in cascades to different finite levels have the same energy, and also using the available spectroscopic data), the $I_{\gamma\gamma}(E_1)$ dependence only on the energy of the primary transition, $E_1$, can be extracted with an acceptable accuracy from the experimental spectrum $I_{\gamma\gamma}(E_\gamma)$. Without this operation, the experimental distribution $I_{\gamma\gamma}(E_\gamma)$ can be accurately described by the infinite number of significantly different functions ρ and Γ because of their correlation. In a small interval, ΔE, of energies $E_1$ of primary transitions, the sum of the intensities of TQC from the initial levels $\lambda$ to the group of low-energy finite levels $f$ through the intermediate levels $i$ can be represented by the equation:

$$I_{\gamma\gamma}(E_1 \pm \Delta E/2)=\sum_{\lambda,f}\sum_{i}\frac{\Gamma_{\lambda i}}{\Gamma_{\lambda}}\frac{\Gamma_{if}}{\Gamma_{i}}=\sum_{\lambda,f}\sum_{j}\frac{\Gamma_{\lambda j}}{<\Gamma_{\lambda j}>M_{\lambda j}}n_j\frac{\Gamma_{jf}}{<\Gamma_{jf}>m_{jf}}. \qquad (4).$$

In the interval ΔE, $n_j=<\rho_j>\cdot\Delta E$ is the number of excited cascade levels, $<\rho_j>$ is the average density of levels of all types, $<\Gamma_{\lambda j}>M_{\lambda j}$ is the sum of partial widths $\Sigma_j\Gamma_{\lambda j}$ of primary transitions to $M_{\lambda j}$ of intermediate levels, $<\Gamma_{jf}>m_{jf}$ is the sum of partial widths $\Sigma_j\Gamma_{jf}$ for secondary transitions to $m_{jf}$ finite levels (since $<\Gamma_{\lambda j}> = \Sigma_j\Gamma_{\lambda j}/M_{\lambda j}$ and $<\Gamma_{jf}> = \Sigma_j\Gamma_{jf}/m_{jf}$).

Since it is impossible to determine parameters of all cascades in experiments, to solve the system of equations (4) in the entire energy range of primary transitions and simultaneously determine ρ and Γ, the experimental intensities $I_{\gamma\gamma}(E_1)$ are approximated using model representations of functions $\rho(E_{ex})=\varphi(p_1,p_2\ldots)$ and $\Gamma(E_1)=\psi(q_1,q_2\ldots)$ for all observed primary gamma-transitions. In all experiments *FWHM*s of the resolved peaks do not exceed 2 – 4 keV.

The inadmissibility of using experimentally unverified representations for $\rho(E_{ex}) = \varphi(p_1,p_2\ldots)$ and $\Gamma(E_1) = \psi(q_1,q_2\ldots)$ was discussed in detail in the previous versions of the data analysis showing that the uncertainty of the parameters ρ and Γ is mostly determined by a systematic error due to inaccuracy of model representations of experimental data. One can estimate the error and

the way to correct the model representations about ρ = $f(p_1, p_2, ..)$ and Γ = φ $(q_1, q_2, \ldots)$ only by comparing various versions of their description.

For model representation of the level density, we used the model of n-quasiparticle nuclear excitations (usually applied in the study of pre-equilibrium reactions in nuclei [10]) and a phenomenological coefficient of an increase in the density of collective levels (balance in the changes of entropy and energy of quasiparticle levels) from the model [11] modified by taking into account a breakup in the Cooper pairs of nucleons. The strength functions of electrical and magnetic transitions were presented, as in the model [12], with the addition of one or two local peaks to accurately describe the experimental distributions $I_{\gamma\gamma}(E_1)$. Studies performed in 2017 confirmed the need to add local peaks to the smooth parts of strength functions and showed that the influence of their different descriptions on the obtained parameters is insignificant.

Even at the initial 'model-free' stage of our method, when the TQC intensities were approximated without any theoretical representations for $\rho(E_{ex})$ and $\Gamma(E_1)$, a step structure was revealed in the $\rho(E_{ex})$ function. Further analysis of the experimental data showed that the level densities are not reproduced with the accuracy of the experiment by the models ignoring the existence of the boson state of nuclear matter. For all investigated nuclei, the presence of steps, probably caused by the breakup of the Cooper pairs in the nucleus, is confirmed by the changes in the representations of $\rho(E_{ex})$ and $\Gamma(E_1)$ introduced by the development of the empirical model. The number of investigated nuclei increases, while the fraction of phenomenological representations of the extracted parameters ρ and Γ is minimized for the verification of the data obtained.

The analysis of new results confirmed the obtained earlier dependence of dynamics of interaction between Fermi and Bose nuclear states on the nucleus shape. In the mass dependence of Cooper pair breaking thresholds (parameters of $\rho(E_{ex})$ function) obtained from the fit, breaking pair thresholds in spherical nuclei ($A < 150$) are higher than in deformed nuclei ($A > 150$). It also follows from the ratios of densities of vibrational and quasi-particle levels that this interaction manifests itself in the neutron binding energy range and probably differs for nuclei with various nucleon parities.

The verification of ρ and Γ obtained in early fits and the estimation of the achieved accuracy of the model were made by comparing experimental gamma-spectra with their calculation from the practical gamma-decay model. The analysis of the sources of systematic errors in ρ and Γ made it possible to conclude about a possible description of spectra of products from any nuclear reaction by the practical model with an accuracy of several percent.

**Investigations of neutron-charged particle reactions**

Experimental and theoretical investigations of neutron-charged particle reactions induced by fast neutrons were carried out. The experiments were conducted at the Van de Graaff accelerators EG-5 in FLNP JINR and EG-4.5 of the Institute of Heavy Ion Physics of Peking University. Data on the neutron reactions with the emission of charged particles induced by fast neutrons are of much interest for studying the mechanisms of nuclear reactions and atomic nuclear structure as well as in choosing engineering materials and in performing calculations in the development of new facilities for nuclear power engineering.

# SCIENTIFIC HIGHLIGHTS

A paper devoted to the study of the $^{144}$Sm(n,α)$^{141}$Nd and $^{66}$Zn(n,α)$^{63}$Ni reactions at $E_n$= 4.0, 5.0 and 6.0 MeV has been published. The data have been obtained for the first time. The experimental values of cross sections are compared with the available libraries and calculations using the TALYS-1.6 code. Our results support the EAF-2010 data and are in good agreement with TENDL-2015.

The cross sections for the $^{10}$B(*n*,t2*α*) three-body reaction and $^{10}$B(*n,α*)$^{7}$Li reaction at $E_n$=4.0, 4.5 and 5.0 MeV were measured. The measurements were performed on the 4.5-MV Van de Graaff accelerator at Peking University. An ionization chamber manufactured at FLNP JINR was used as a detector. A new system for acquisition and accumulation of experimental data developed on the basis of a high-speed digitizer, was employed. Due to the fact that there are several channels of the reaction with emission of a triton and two α-particles, detailed calculations were made for analyzing the experimental data. As an example, **Figure I-3-10** shows an amplitude spectrum of events from the region of effective events and time window of multidimensional experimental spectrum at $E_n$ = 4.0 MeV.

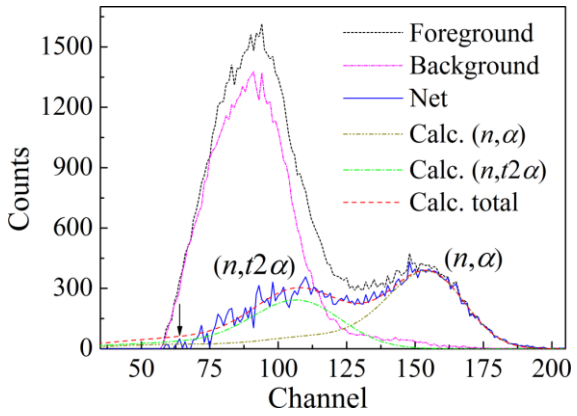


*Fig. I-3-10. Amplitude spectrum of events from the region of effective events and time window of multidimensional experimental spectrum at $E_n$ = 4.0 MeV.*

The results on the cross sections and errors of the measurements of the $^{10}$B(*n*,t2*α*) and $^{10}$B(*n,α*)$^{7}$Li reactions are given in **Fig. I-3-11** and **Table I-3-I**.

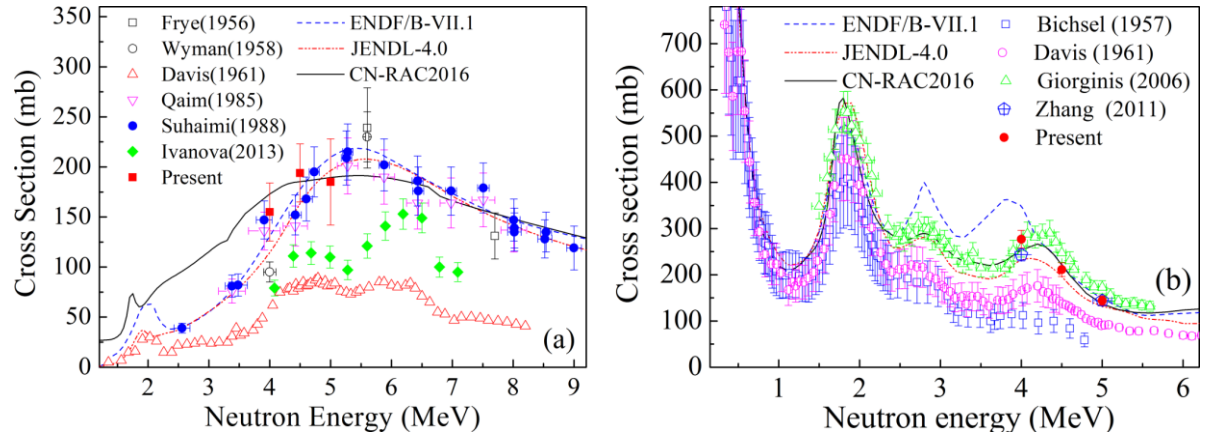


*Fig. I-3-11. Our results on cross-sections in comparison with previous measurements and data libraries: a) for $^{10}$B(n,t2α) reaction and b) for $^{10}$B(n,α)$^{7}$Li reaction.*

**Table I-3-I**. Measured cross sections for $^{10}B(n,t\,2\alpha)$ and $^{10}B(n,\alpha)^{7}Li$ reactions.

| $E_n$ (MeV) | $\sigma(n,t\,2\alpha)$ (mb) | $\sigma(n,\alpha)$ (mb) | | | |
|---|---|---|---|---|---|
| | | Total | Leaking | Forward $\alpha$ | Backward $\alpha$ |
| 4.0 | 155 (19%) | 277 (7%) | 35 (9%) | 143 (11%) | 99 (9%) |
| 4.5 | 194 (15%) | 211 (7%) | 30 (10%) | 107 (11%) | 74 (9%) |
| 5.0 | 185 (23%) | 144 (7%) | 22 (10%) | 72 (12%) | 50 (9%) |

**Investigations of nuclear reactions induced by gamma-rays and fast protons**

Work was carried out to estimate cross sections, isomeric ratios, and other effects in nuclear reactions with neutron yield induced by photons and fast protons. The calculations were made using the Talys software and own computer codes. The Talys software system is intended to determine nuclear reaction cross sections and the structure of the atomic nucleus and operates mainly under Linux with a simple and efficient interface.

Cross sections, isomer relations, forward-backward asymmetries and other parameters of (γ, n), (γ, p), (α, γ), (α, n), (p, n) reactions on isotopes of Sn, Sm, In and other nuclei were obtained. The theoretical estimates were compared with the literature experimental data, and a good agreement was found. Addtional nuclear data such as parameters of the nuclear potential, nuclear state and level densities were detetermined.

The obtained theoretical estimates may find application in both fundamental and applied areas of nuclear physics. From the fundamental point of view, the results can be useful in studies of mechanisms of nuclear reactions, structure of nucleus, and astrophysical problems. Regarding applied problems, the nuclear data may be helpful for obtaining new isotopes for medicine, electronics and industry, as well as for improving gamma-ray activation methods and creating new neutron sources.

These estimates and calculations were done to develop and continue programs on nuclear data at the basic facilities of FLNP JINR including the IBR-2 research reactor, new neutron source IREN and electrostatic generator EG-5.

**Activities within the n_TOF collaboration, CERN**

In 2017, within the framework of the TOF-collaboration at CERN with the participation of FLNP specialists, the precision measurements of the neutron capture cross section of fissioning nuclei $^{235,\ 236,\ 238}U$ [13-15], $^{240}Pu$ [16] and $^{241}Am$ [17] were performed for a wide range of neutron energies. This work is necessary for the design and licensing of a new generation of nuclear reactors. The experiments were carried out with isotope targets $^{7}Be$ [18] and $^{33}S$ [19], which are important for clarifying the nucleosynthesis scenario.

**Activities within the framework of TANGRA project**

***Determination of physical characteristics of gamma-detectors and optimal geometry of BGO-based detector system***

In 2017, the detector system of the TANGRA facility was upgraded, which involved the replacement of gamma-ray detectors based on NaI crystals with more efficient BGO crystal detectors. Each detector is a scintillation assembly consisting of a BGO crystal (76 mm in diameter and 65 mm thick) and Hamamatsu R1307 photomultiplier. In total, there are 24 detectors which can be arranged in different geometric configurations relative to the target depending on the problem being solved.

The physical characteristics of the system, such as resolution, efficiency, optimum operating voltage for the new detectors were tested.

To determine the operating voltage and test each detector of the new system, a specialized test setup was constructed (**Fig. I-3-12**). Calibration sources $^{137}Cs$ ($E_\gamma$ – 662 keV), $^{60}Co$ ($E_\gamma$ – 1127 keV and 1332 keV) were placed in the center. The voltage was varied from 800 to 1500 V; the upper limit was selected according to the photomultiplier specifications.

***Fig. I-3-12.*** *First test geometry for BGO-based detectors.*

The optimum operating voltages at the photomultipliers of all detectors were selected on the basis of the experimentally obtained dependences of the amplitude of detector signals on the applied high voltage. The energy and time resolution of the detectors were also determined for the energies of gamma-rays emitted by the calibration sources and for the lines of $^{12}C$ (4.43 MeV), $^{14}N$ (5.1 MeV) and $^{16}O$ (6.13 MeV).

To determine the optimal geometric configuration of detector arrangement, various configuration variants were tested. **Figures I-3-13 and I-3-14** show different configuration variants with 10 detectors with and without a collimator.

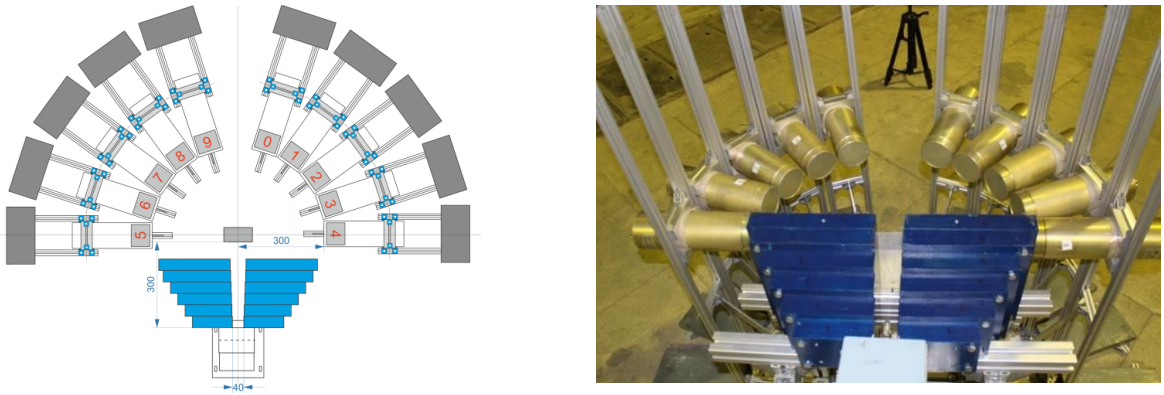


***Fig. I-3-13.*** *System with 10 detectors, configuration variant "A" – compact geometry with a collimator.*

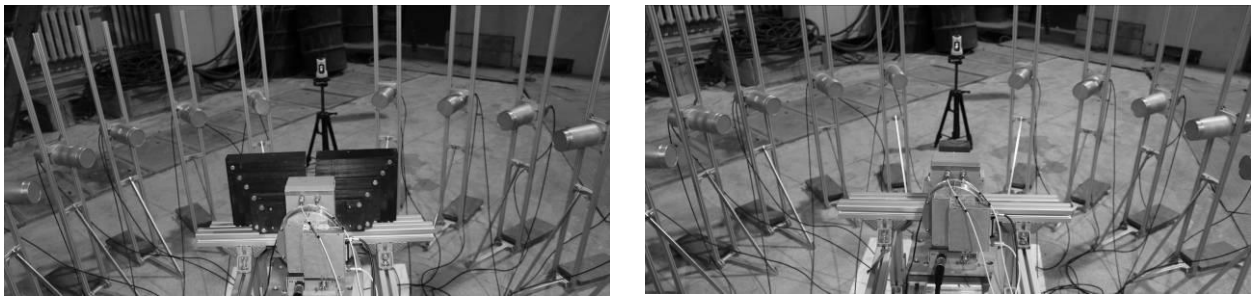

a) b)

***Fig. I-3-14.*** a) *System with 10 detectors, configuration variant "B" – compact geometry with a collimator, detectors are located at a distance of 100 cm from the sample position; b) System with 10 detectors, configuration variant "C" – compact geometry without a collimator, detectors are located at a distance of 100 cm from the sample position.*

The result of the test measurements with a carbon target for three presented variants is shown in **Fig. I-3-15**.

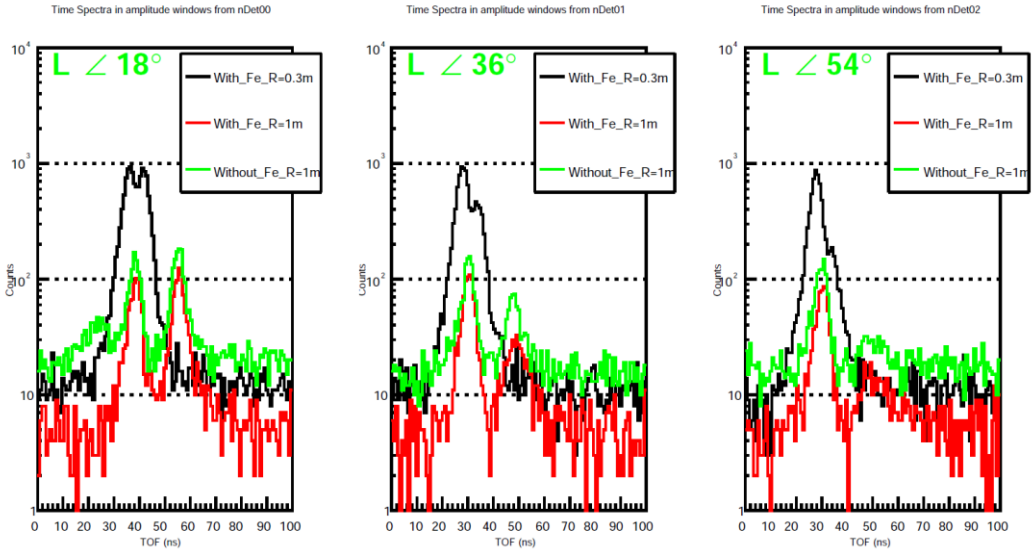


***Fig. I-3-15.*** *Time spectra of signals coming from gamma-detectors.*

It can be seen from the figure that at a target-to-detector distance of 100 cm (green and red curves), the time-of-flight separation of neutrons and gamma-rays is much better than for the compact arrangement of the detectors (black curve). But the number of events registered during the same time period decreases by almost an order of magnitude. At the same time, the comparison of measurements for a distance of 100 cm with and without a collimator (red and green curves) shows that at such large distances the collimator is no longer needed. This allows one to position the target under study as close as possible to the neutron generator, thus achieving a gain in statistics due to a higher neutron flux on the target. Further test measurements together with simulations showed that the detector-sample distance of 65 cm is sufficient for effective separation of neutrons and gamma-rays by time of flight, while the statistics acquisition rate increases by almost an order of magnitude as compared to the old configuration with NaI-based detectors. The

final geometry of the facility involves the use of 36 tagged neutron beams and 18 BGO-detectors (**Fig. I-3-16**).

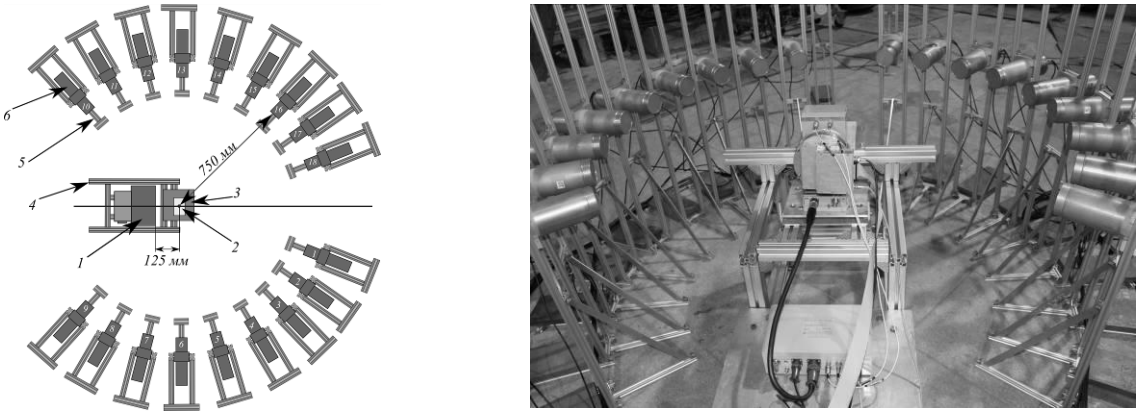


***Fig. I-3-16.*** *Schematic of TANGRA experimental facility: 1 – generator ING-27, 2 – target, 3 – target holder, 4 – aluminum frame, 5 – support for gamma-ray detector, 6 – gamma-ray detector.*

***Determination of the position of a tritium target and direction of tagged neutron beams using a 2D silicon strip detector***

One of the criteria of correct measurement of neutron beam profiles can be the experimental determination of the position of a tritium target in the ING-27 neutron generator, as well as the comparison of the obtained results with the specification data stated in the generator certificate. A 2D strip silicon profilometer consisting of 16 crossed strips (8 vertical and 8 horizontal strips) producing 64 square zones (pixels) with sides of 15 mm was used as a neutron detector. The detector and preamplifiers were placed in an aluminum housing equipped with a support, which makes it possible to easily move the profilometer in vertical and longitudinal directions. The neutron detection by the profilometer is done by detecting protons and alpha particles produced in the reactions $^{28}$Si($n,\alpha$)$^{25}$Mg (reaction energy threshold $B_\alpha$ = 9.985 MeV) and $^{28}$Si($n,p$)$^{28}$Al ($B_p$ = 11.586 MeV), which, in its turn, imposes restrictions on the minimum energy of detected neutrons.

To accomplish this task, a number of measurements were made, in which the distances from the end face of the ING-27 neutron generator to the profilometer varied in the direction of the neutron beam, Z. **Figure I-3-17a** shows the distribution of tagged beams obtained at a distance of 10 cm from the generator. When the distance from the generator to the profilometer is changed, this distribution also changes, which makes it possible to plot the position of the centroid of the tagged beam (**Fig. I-3-17b**) as a function of the distance and thus determine the trajectories of neutrons composing the tagged beam. The result of this procedure for one Y-coordinate is presented in **Fig. I-3-17c**.

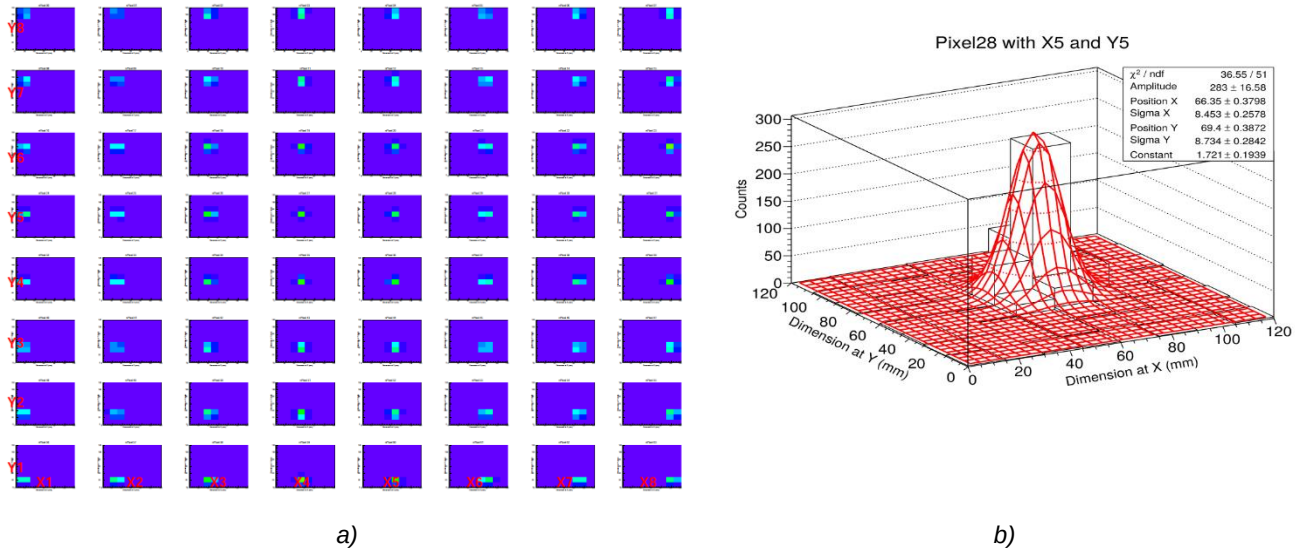


*a)* *b)*

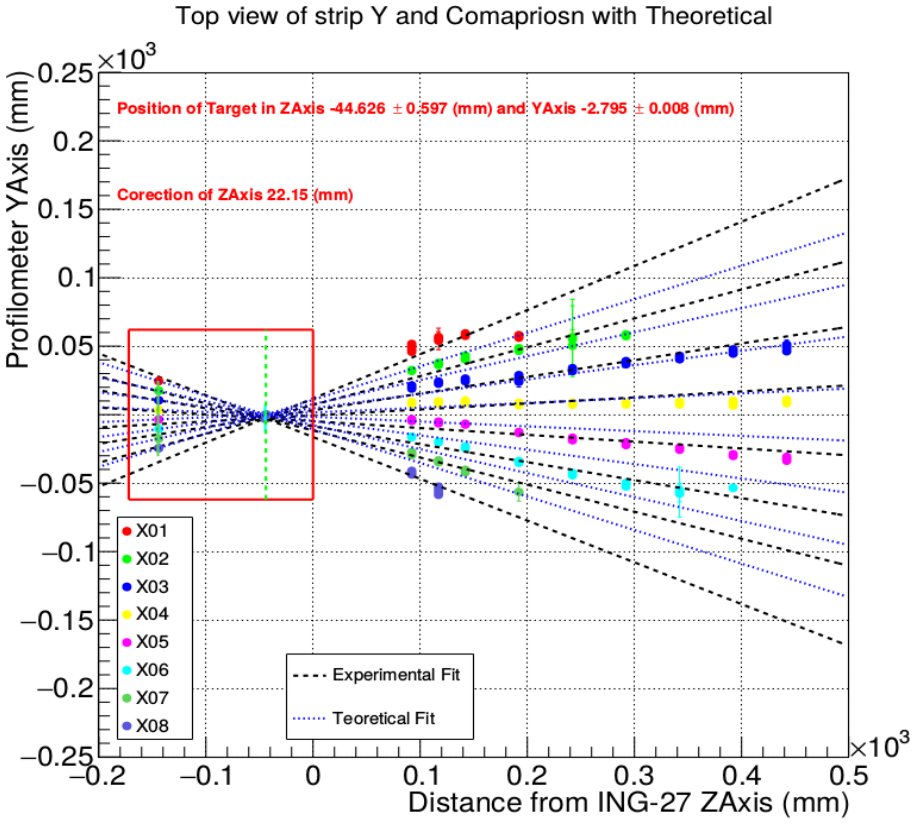


*c)*

***Fig. I-3-17.*** a) Distribution of tagged beam profiles obtained in the described experiment. b) 2D approximation of position of tagged beam. c) Neutron trajectories estimated by centroids of tagged beams in XZ plane (X-strips are summed).

***Calculation of angular distribution of gamma-radiation emitted in the process of inelastic neutron scattering by atomic nuclei***

The search for a correct theoretical description of angular distributions of gamma-rays emitted by nuclei as a result of inelastic neutron scattering is an important problem to be solved in the course of studying inelastic neutron scattering. The available experimental data differ from each other quite a lot, and theoretical predictions could significantly improve the situation in this area. In addition, information on the relationship between the easy-to-measure angular distribution of gamma-rays and properties of the nucleus is of importance for obtaining information about the nuclear structure.

The process of inelastic neutron scattering by nuclei can be described in two fundamentally different approaches, namely using the direct reaction approximation or the compound nucleus approximation.

As a "first step", it was decided to perform calculations within the framework of the compound nucleus model, because, first, this approach is much better described in the literature than the alternative model, and, second, there is evidence of "impurity" in the complex mechanism of the scattering of fast neutrons by light nuclei [20].

To calculate the angular distribution of gamma-rays emitted in inelastic scattering, the following model was proposed: a neutron hits the target nucleus, which captures the neutron and as a result, makes a transition to an excited state; then it emits a neutron, and the residual excitation is removed by emitting a gamma-ray. The scheme of this process is shown in **Fig. I-3-18**.

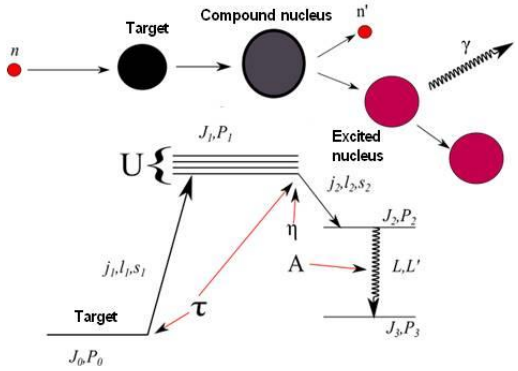


***Fig. I-3-18.*** *Scheme of inelastic scattering process.*

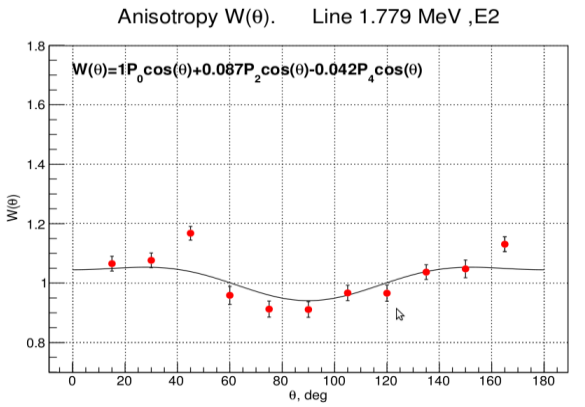


***Fig. I-3-19.*** *Comparison of the results of calculations with experimental data for $^{28}Si$, $E_\gamma$ = 1.779 MeV, transition E2.*

The results obtained for light nuclei are in poor agreement with the experimental data (**Fig. I-3-19**), which, in principle, is expected, since the fraction of processes which occur with the formation of compound nuclei is small for light nuclei.

**Measurements of the probability of small heating and total losses of UCN on the surface of Fomblin oil**

New processing of the results from the measurements (made by us in 2011-2015) aimed at studying the UCN interaction with the surface of Fomblin oil was performed. The new processing gave a higher accuracy in determining the probability of small heating on Fomblin.

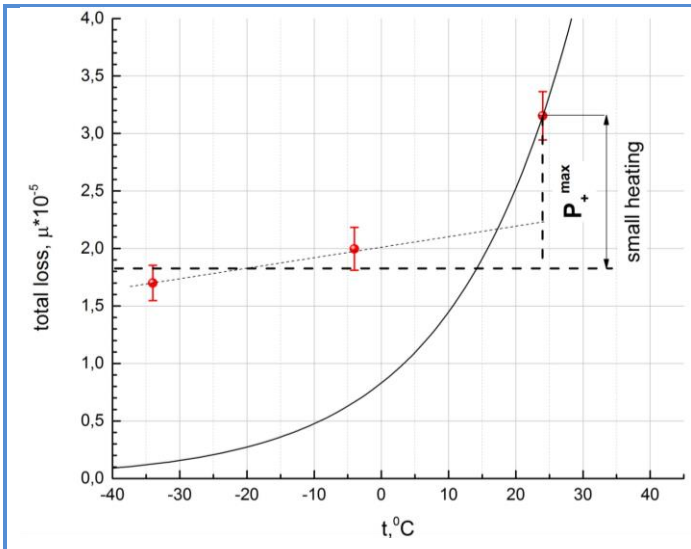


***Fig. I-3-20.*** *Upper limit of probability of UCN small heating on Fomblin. Red points follow the temperature dependence of total UCN losses; solid line shows the temperature dependence of probability of UCN small heating.*

The main result is the following: if earlier, when measuring the probability of small heating, we could speak only about its lower limit, now, on the basis of the comparison of the results from these measurements with the probability of total UCN losses, one can also speak about the upper limit of the probability of small heating (**Fig. I-3-20**).

The probability of small heating of UCN on Fomblin at 240°C is in the range of $(1.05 \pm 0.02_{stat}) \times 10^{-5} - (1.31 \pm 0.24_{stat}) \times 10^{-5}$. In addition, it can be stated that since the spectra of heated UCN are the same for all the substances measured, the upper limit of the probability of small heating for all these substances is about 1.3 times higher than the lower limit.

**Development and manufacturing of a $^{10}$B monitor of thermal neutrons**

The putting into operation of a new type of UCN source being developed by a group of FLNP specialists will make it possible to increase the UCN flux density by three orders of magnitude in comparison with the existing sources. In particular, this will provide higher accuracy for measurements in the traditional for UCN experiments. For example, it will be possible to measure the neutron lifetime with accuracy better than 0.1 s. An increase in the statistical accuracy requires more attention to systematic errors of measurements. One of the sources of systematic errors in the measurements with UCN is the detection systems used.

For UCN detection, proportional $^{3}$He-gas counters with a thin entrance window of Al or Ti (often with a seal made of polymeric materials) are usually used. Our studies have shown that $^{3}$He can diffuse through the polymeric seals of the windows and get into the UCN storage volume. This can lead to systematic errors in the measurements, which are difficult to be taken into account. A UCN detector with Teflon seal can lose up to 15% of $^{3}$He per year, with Viton seal - up to 3% of $^{3}$He per year. Metal window seals are also not reliable enough, because can lead to microdamages of window foils.

A radical solution of the problem of $^3$He penetration into the UCN storage volume is the replacement of $^3$He with another sensitive element.

The existing UCN detectors usually have a thickness of ~ 5 cm, small number of wires and use charge-sensitive preamplifiers. They provide a maximum count rate of ~$10^3$-$10^4$ $s^{-1}$. For the new UCN source, it should be increased by two-three orders of magnitude.

To test the manufacturing technology and verify the specified characteristics of such a detector, we designed and manufactured a thermal neutron monitor with $^{10}$B sputtered on the rear wall. The monitor is a multiwire proportional gas counter coated with $B_4C$ ($^{10}$B enrichment 85%) with a thickness of 0.2 μm. The thickness of the working area of the monitor is 12 mm. The reaction used to detect neutrons is:

$$^{10}B+n \rightarrow^{(93.7\%)} \alpha(1.47MeV) + {}^{7}Li(0.84Mev) + \gamma(0.48MeV)$$
$$\rightarrow^{(6.3\%)} \alpha(1.78MeV) + {}^{7}Li(1.01MeV) \qquad \sigma = 3835\ b$$

The detection efficiency for neutrons with a wavelength of $\lambda$ = 2 Å is $1\times10^{-2}$, which provides the probability of UCN detection close to 100%. It was shown that a monitor equipped with a fast current preamplifier can provide a count rate of up to $10^6$ $s^{-1}$.

**Neutron diffraction by a moving grating**

In the FLNP Annual Report for 2016, we reported about the experiment carried out at the Institute of Laue-Langevin that year. Its purpose was to verify the theoretical prediction that at a certain height of the profile of a moving grating a substantial suppression of the zero-order diffraction is possible with a corresponding increase in the intensity of the peaks of other orders. If this prediction is true, then one can increase the efficiency of energy transfer to the neutron during diffraction on a moving grating by choosing the grating profile.

A new grating, prepared as before, on the periphery of a silicon disk had 84000 radial grooves with a profile depth of 0.22 μm, in contrast to the previously used grating with a profile depth of 0.14 μm.

Basing on the results of the study of the grating profile by atomic force microscopy (ACM) reported in 2016, we indicated that the teeth and grooves of this grating have not a rectangular but a substantially trapezoidal profile. The comparison with the spectrum obtained for a grating with a smaller profile depth supported the prediction that the zero-order intensity can be significantly suppressed (**Fig. I-3-21**). This was the main result of this experiment.

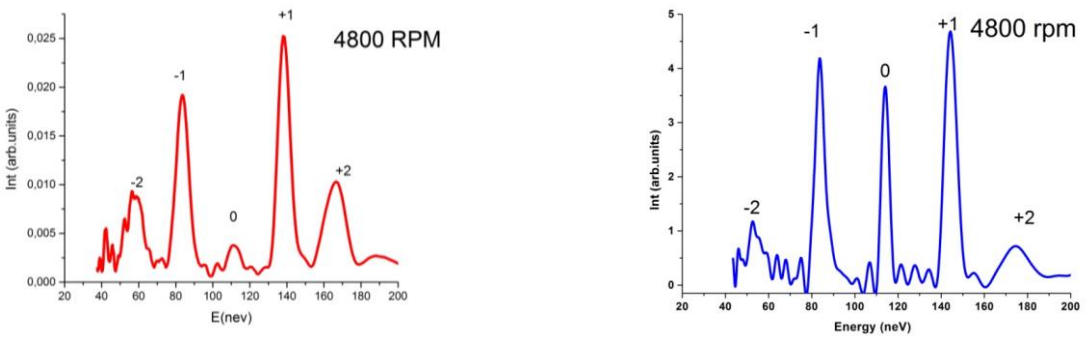


***Fig. I-3-21.*** *Neutron diffraction spectra from a moving deep-profile grating (at the left) in comparison with the previously measured spectrum for a grating with a smaller profile depth (at the right). It can be seen that the zero-order intensities differ significanlty.*

At the same time, the experimental spectra were not in satisfactory agreement with the results of the calculation based on the AFM data. The reason for this discrepancy was not entirely clear, and, as noted in the report, a more detailed analysis was required to clarify it. In 2017, the corresponding work was carried out, which enabled us to answer previously raised questions.

First, the analysis of the AFM data and consultations with specialists brought us to the conclusion that the data most likely were erroneous. Repeated measurements with the same AFM in ESRF (Grenoble) yielded different results, and the source of the previous methodological error was found. The new results showed that the grating profile is much closer to a rectangular one than was previously thought.

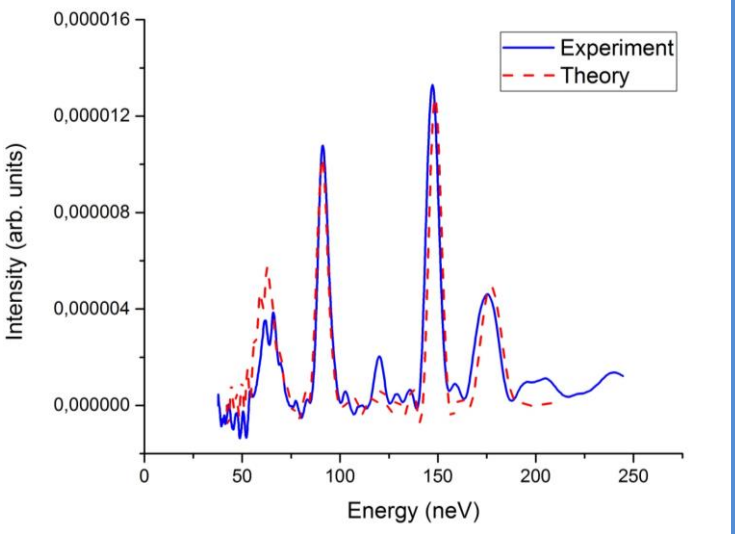


***Fig. I-3-22.*** *Results of the experiment of 2016 and results of the detailed simulations based on new data on the grating and diffractometer.*

Second, we performed detailed Monte-Carlo simulations, which made it possible to reveal a number of systematic effects of the time-of-flight Fourier diffractometer used in the experiment. The detailed simulation of the experiment based on the dynamic theory of diffraction from a moving grating, new AFM data and realistic diffractometer parameters led us to the result that was in satisfactory agreement with the experiment (**Fig. I-3-22**). Thus, all the uncertainties in the interpretation of the experiment of 2016 were removed.

**Preparation of the experiment on the observation of the interaction of UCN with an oscillating barrier under giant accelerations**

The purpose of the upcoming experiment is to check up the validity of the model of the effective potential under giant accelerations of the sample. An important step in the preparation of the experiment is quantum calculations of the interaction of the neutron wave packet with a potential structure oscillating in space at different magnitudes of the maximum acceleration of the object $w_{max} = A(2\pi f)^2$, where A and f are the oscillation amplitude and frequency, respectively.

***Design of sample-resonator***

The realization of the experiment requires samples with the surface oscillating at a frequency of the order of 2 MHz without significant deformation. To solve this problem, an approach employing a bulk half-wave quartz resonator was used. The resonator is a quartz plate about 3 cm in diameter and 270 μm thick, which corresponds to half the wavelength of ultrasound in quartz. Thin aluminum films serving as electrodes are deposited on flat surfaces of the resonator. When the alternating voltage is applied to the electrodes, the sample is deformed, and the deformation value reaches its maximum in resonance. The amplitude-frequency characteristic of the sample

has a rather complex structure, which is indicative of the presence of multiple oscillation modes.

In 2017, for experimental investigations of the resonator, a special stand—vibrometer—for mapping the surface of an oscillating sample was constructed (**Fig. I-3-23**). It consists of a laser interferometer and two-coordinate table. For successful operation of the device and the analysis of the results, special computer software was developed. The device allows us to measure the shape of the surface in simultaneous synchronization with the phase of the sample movement. The measurement of the surface profile of the resonator oscillating at a resonant frequency of the order of 2.1 MHz showed that the sample surface does not remain flat and various fragments of the sample oscillate in antiphase forming a complex spatial structure (**Fig. I-3-23**).

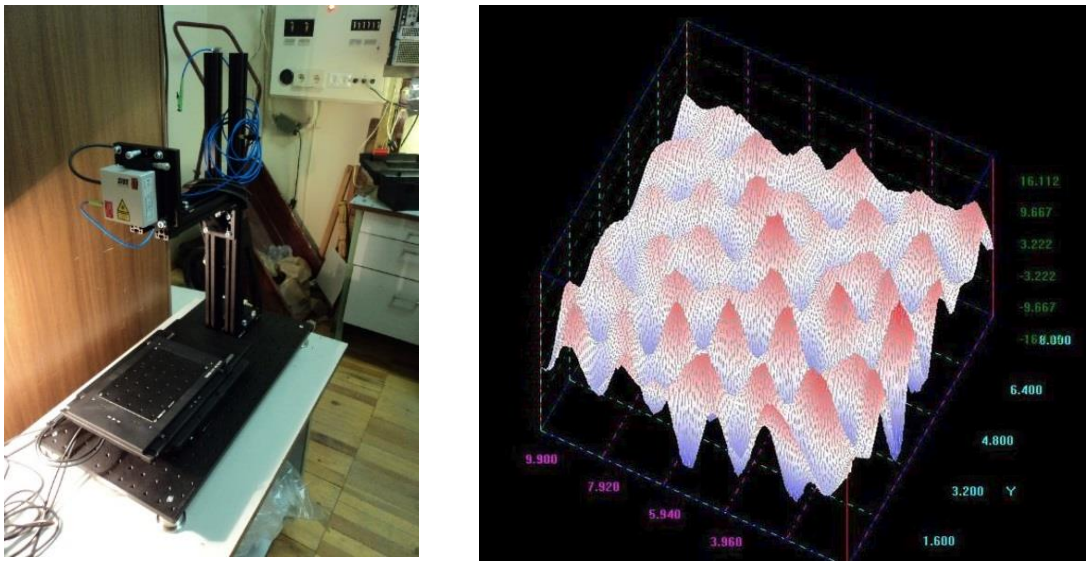


***Fig. I-3-23.*** *2D laser vibrometer (at the left) and instantaneous state of the resonator surface oscillating at 2.1 MHz.*

At present, the possibility for computer calculations of the deformation of piezoelectric resonators is considered, which is quite a challenge. These calculations will make it possible to find the best sample configuration.

***Quantum calculations of nonstationary neutron-optical effects***

In parallel with the work on the creation of the sample, we carried out investigation of UCN interaction with a potential structure oscillating in space with a high frequency. In the absence of the theory of dispersion of neutron waves in an accelerating substance, a quantum nonstationary problem of neutron interaction with an oscillating potential structure, based on the ordinary dispersion law is under study. Since it was previously shown that in the simple case of an oscillating potential barrier oscillating with the necessary frequency and amplitude, the non-stationary effects for the transmitted state are very small, we considered an approach in which neutrons pass through an oscillating resonance structure consisting of two barriers with a well between them.

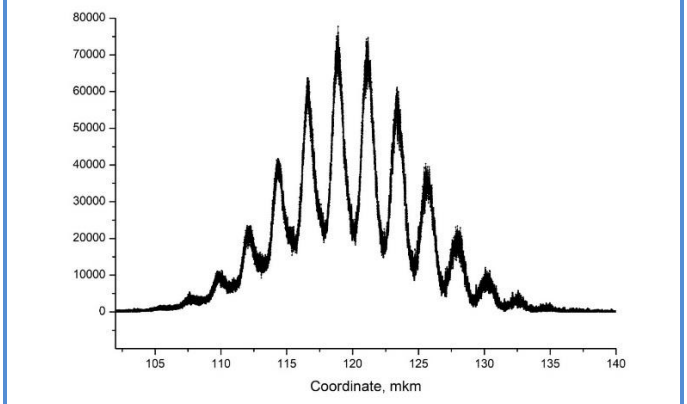


*Fig. I-3-24. Structure of a wave packet after passing through a resonance structure oscillating in space. Results of quantum calculations.*

Calculations based on the method of splitting the evolution operator demonstrated again significant oscillation of the neutron flux passing through such a structure (**Fig. I-3-24**). This geometry was selected as a priority for further research.

At the same time, the analysis of the obtained results has raised a number of questions. At present, it is not entirely clear whether they are connected with the calculation errors or are a manifestation of not yet fully understood details of the phenomenon. The work will be continued using the resources of the LIT JINR cluster (Hybrilit).

**Neutron diffraction from surface ultrasonic waves**

Previously in 2017, in collaboration with IPTM RAS (Chernogolovka) and the Max Planck Institute (Munich, Germany), an experiment was performed to observe neutron diffraction from surface ultrasonic waves. This work extended a relatively short list of non-stationary quantum experiments with neutrons.

In 2017, considerable theoretical work was done to study the diffraction of neutron waves from stationary and moving gratings with a sinusoidal profile, as well as also from a standing surface wave.

**Applied research**

***Application of resonance neutrons for the search for palladium in the engine components of the Proton rocket***

The IREN facility makes it possible to perform time-of-flight experiments to determine the elemental and isotopic composition of samples by characteristic neutron resonances. The cross section for the interaction of neutrons with matter in the neutron energy region from fractions of eV to hundreds of keV has a pronounced resonance structure, and the position of neutron resonances, as well as their intensity (the area under the resonance) are unique for each element, which allows us to identify various elements and their isotopes with high accuracy. The sensitivity of the method is different for different elements and depends on a number of factors (the presence of resonances in the required energy region, neutron cross-section value in resonances, presence of background resonances from other elements in the same region, etc.). Neutrons have great penetrating power; therefore, the method makes it possible to analyze rather massive samples and requires no preliminary preparation, cutting, etc.

Palladium is one of the elements for which the resonance method works particularly well, because for this element very strong resonances are observed in the energy range up to 100 eV

(where the sensitivity of the method is high), which makes it possible to determine the presence of palladium even in very small amounts.

In the experiment, we investigated gas generator components of the engine of the second and third stages of a Proton heavy-lift rocket, comprising soldering with a significant content of palladium. The presence of palladium in these components is an indicator of faults in the technological process of manufacturing of the engine, which can lead to an accident. To detect palladium in the samples provided by Roscosmos, they were placed in a neutron beam inside the "ROMASHKA" scintillation spectrometer consisting of 24 NaI(Tl) crystals.

First we made measurements with a sample consisting of pure metallic palladium. **Figure I-3-25** shows a time-of-flight spectrum of a 5-g palladium sample, which was obtained at our facility at a measurement time of 1 hour. The observed resonances correspond to the known tabulated values for various palladium isotopes.

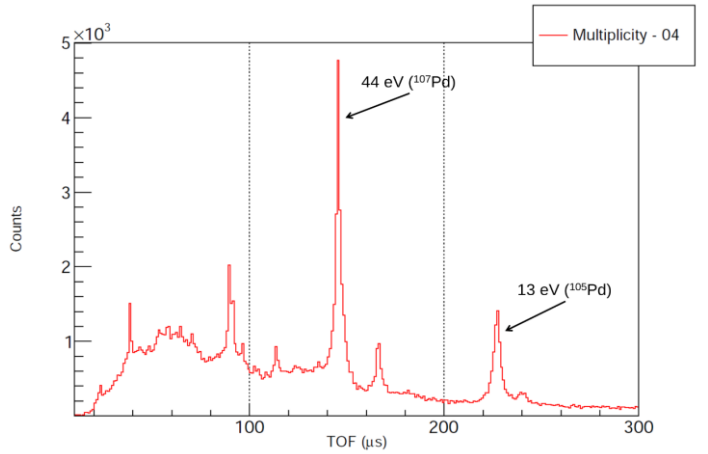


***Fig. I-3-25.*** *TOF spectrum of a palladium sample with a mass of 5 g.*

The measurements were carried out at a flight path of 11.2 m. The operating mode of the IREN facility: pulse repetition rate – 25 Hz, electron pulse duration ~ 100 ns, peak beam current – 1-1.5 A, electron energy ~ 50 MeV. The integral neutron yield is ~ $3 \cdot 10^{11}$ $s^{-1}$. To control the neutron flux intensity, we used a neutron counter placed directly at the beam entrance to the experimental hall.

To test the possibility of determining the presence of a palladium-containing solder by this method, we used two parts of the sample (about 60 g each) provided by Roscosmos. The palladium-containing solder was found only in sample 1. The presence of palladium in sample 1 and its absence in sample 2 were tested by X-ray fluorescence analysis at the Institute of Physical and Technical Problems.

To detect gamma rays emitted by the irradiated target, we used a system of 24 NaI(Tl) gamma-spectrometers (“ROMASHKA"). To reduce the number of neutrons arriving at gamma-detectors, a cylinder of boron carbide was installed inside the "ROMASHKA" setup. In addition, for the same purpose a collimator made of borated polyethylene was placed immediately in front of the entry point of the neutron beam. The irradiated samples were suspended in the center of the detector system.

**Figure I-3-26** presents time-of-flight spectra for various multiplicities of gamma-rays recorded by the "ROMASHKA" detector system for different samples.

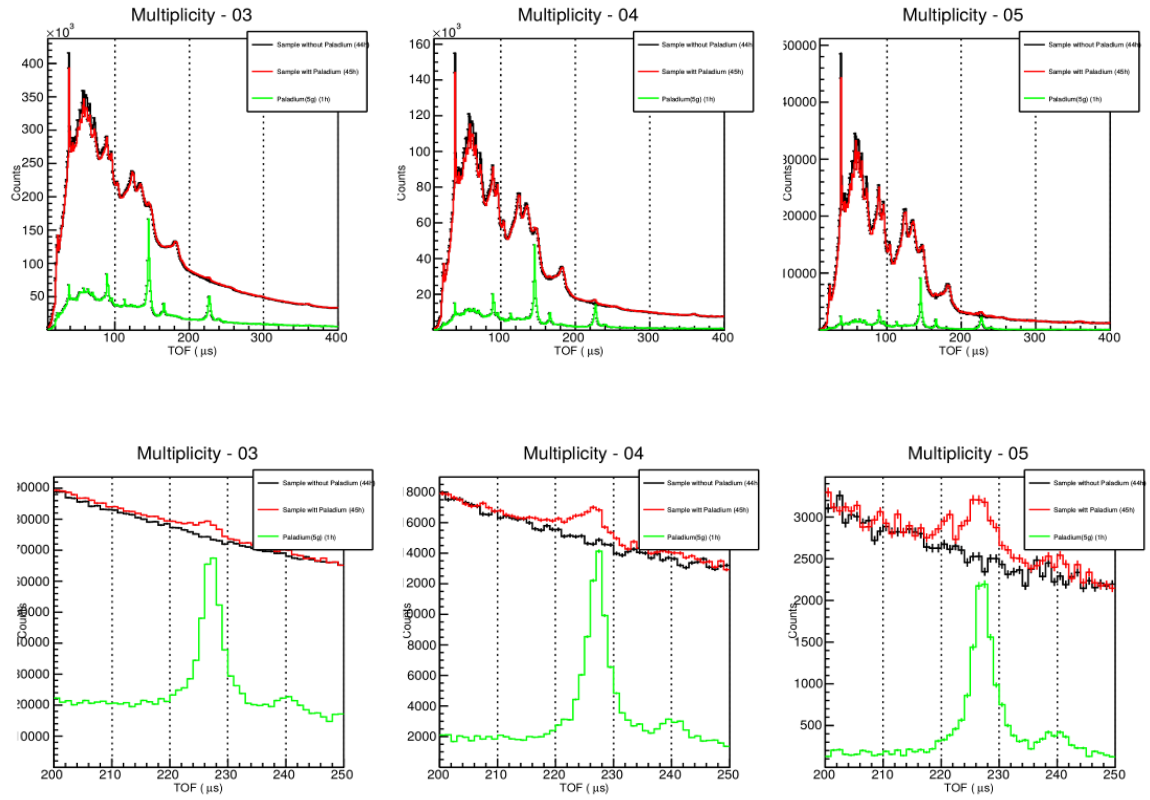


***Fig. I-3-26.*** *Top: time-of-flight spectra for various gamma-ray multiplicities corresponding to the analyzed samples: with palladium No. 1 (red), without palladium No. 2 (black) and pure palladium (green). Bottom: parts of spectra in the palladium resonance region of 13 eV.*

These spectra demonstrate that the technique can reliably diagnose the amount of palladium of the order of 100 mg in samples of about 60 g.

***Application of the neutron resonance analysis method to investigate the elemental composition of archaeological finds***

In 2017, at the IREN facility, experiments were carried out to determine the elemental composition of a number of archaeological atrefacts provided by the Institute of Archeology, RAS (**Figs. I-3-27a**, I-**3-28a**, I-**3-29**). The studies were done using the neutron resonance capture analysis (NRCA), the main principles of which are described in [21] and in the previous section. A large liquid scintillation detector was used as a γ-ray detector [21].The measurements were made at a 60-m flight path of IREN beamline 3. Some time-of-flight spectra obtained in the measurements are shown in **Fig. I-3-27b** and I-**3-28b**.

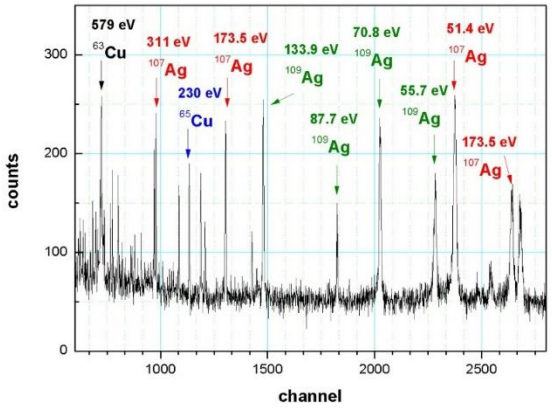


***a)*** ***b)***

***Fig. I-3-27.*** *a) Coins (Bosporus staters) from the Phanagoria's treasure (3rd century AD).b) Part of the time-of-flight spectrum from the radiative capture of neutrons obtained in measurements with coins from the Phanagoria's treasure.*

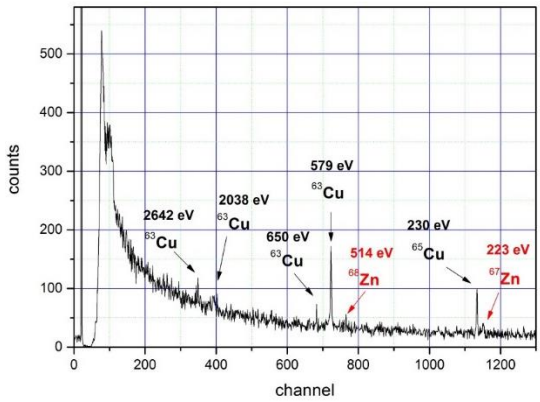


***a)*** ***b)***

***Fig. I-3-28.*** *a) Fibula from the Podbolotievsky burial ground, Vladimir region (10th century AD). b) Part of the time-of-flight spectrum from the radiative capture of neutrons obtained in measurements with a fibula.*


***Fig. I-3-29.*** *A silver medallion and zoomorphic figurine (information on the location and age of the finds have not yet been provided).*

For the quantitative determination of elements in the objects under study we used a relative method — additional measurements were made with samples with the known parameters, containing the identified elements. The preliminary results on the study of staters and fibula are presented in **Table I-3-II**.

**Table I-3-II**. The content of elements from time-of-flight spectra of the objects under study.

| | Weight, g | Cu, g | Zn, g | Ag, g | Au, g |
|---|---|---|---|---|---|
| Coins | 73.033 | 62.0 ± 3.1 | - | 6.762 ± 0.086 | - |
| Fibula | 19.98 | 13.5 ± 1.5 | 1.06 ± 0.39 | - | 0.0171 ± 0.0027 |

The errors listed in Table II take account of only statistics of registered events. At present, studies are underway to identify possible sources of systematic errors in the analysis and estimate their values.

The applied analytical research method is quite new for FLNP. However, as can be seen from the preliminary results, it could find application in the study of unique objects of archeology and cultural heritage, since it is absolutely non-destructive, requires no special sample preparation procedures (for example, cleaning from patina), and leaves practically no induced radioactivity in objects under study.

***Analysis of human remains from the necropolises of the Moscow Kremlin***

A neutron activation analysis (NAA) of three samples of human remains of the 16th and 17th centuries from the necropolises of the Moscow Kremlin has been carried out at FLNP JINR. The samples were irradiated at two facilities: the IREN source of resonance neutrons and the IBR-2 reactor. Spectra of the induced activity of the irradiated samples were measured using the automatic measurement system developed in FLNP JINR. This system consists of a high-purity germanium detector with spectrometric electronics, a sample changer, and control software. Mass fraction of arsenic, mercury, and some other elements were calculated using two NAA methods—relative and absolute (**Table I-3-III**).

**Table I-3-III.** Mass fractions of arsenic and mercury in the samples.

| № sample | Arsenic (As) | | Mercury (Hg) | |
|---|---|---|---|---|
| | Mass fraction, mg/kg | Relative error, % | Mass fraction, mg/kg | Relative error, % |
| 1 | 0,19 | 30 | 0,36 | 19,1 |
| 2 | 0,23 | 30 | 0,2 | 29,5 |
| 3 | 1,18 | 18,3 | 46,6 | 2,5 |

The obtained values confirm the fact of acute mercury poisoning of Anastasia Romanovna, the first wife of Tsar Ivan the Terrible (sample 3, fragment of hair). High levels of mercury were detected in the bone remains of Tsarevich Ivan Ivanovich (sample 1, **Fig.I-3-30**), the son of Tsar Ivan the Terrible, and Prince Mikhail Vasil'evich Skopin-Shuiskii (sample 2).

*Fig. I-3-30. Sample №1 after cleaning.*

The results provide an opportunity to introduce into scientific circulation the exact values of mass fraction of mercury, arsenic, and other elements in the samples taken from the burials of the Russian historical figures of the second half of 16th–early 17th century.

***Analytical investigations at the IBR-2 reactor***

In 2017, the REGATA facility was used for multi-element instrumental neutron activation analysis of about 1900 environmental samples (vegetation, soil, air filters), a number of technological, biological and archaeological samples, as well as of samples of extraterrestrial origin in the framework of programs and grants of the JINR Member States and Protocols on scientific and technical cooperation with the JINR Non-Member States. Investigations of test samples were conducted for an interlaboratory comparison of the results under the IAEA program. The elemental analysis of ~ 500 samples were performed using a *Thermo Scientific iCE 3500 Atomic Absorption Spectrometer*.

***Development of the NAA&AR experimental base at IBR-2***

In order to replace aluminum transport containers with containers with less induced radioactivity, new materials were tested by irradiating them in pneumatic transport systems and vertical channels of the reactor. In addition, materials with a sufficiently high radiation resistance and low gamma background of induced radioactivity were chosen to replace the aluminum foil currently used as a packaging material for long radiation exposure. Trial batches of transport containers made of PTFE 40 and various modifications of polyetheretherketone (PEEK) were manufactured. Containers made of PTFE 40 were irradiated for 5 hours, and of PEEK – for 30 hours without significant changes in mechanical properties and, obviously, this is not the limit.

A deionizer and specialized laboratory glassware washer were installed and put into operation for preparation of samples for the atomic absorption spectrometer.

On a low-background detector, long-term measurements of background were conducted to determine possible ways to reduce it. The work is carried out in cooperation with the specialists from Comenius University (Bratislava, Slovakia). To verify the correctness of the calculation of the detector efficiency for different sample geometries, a contract was concluded with VNIIM (St. Petersburg) to manufacture volumetric radioactivity standards.

Work has started on the preparation of documents for gaining accreditation of research activities using NAA. The upgrade of the software for automation of NAA on the basis of the accumulated operational experience is in progress and includes the following steps:

- Several new functions that simplify working with experimental data were added to the "NAA Database" program;
- ClosedXML library was imported to the concentration calculation program to link Microsoft Excel directly with the results of the program;
- FTP-server was reinstalled with the CentOS7 Unix system, which allowed more delicate adjustment of experimental data backup;
- The measurement program is being transferred to the VCS technology, which uses the git version control system and allows flexible versioning of the code to fully control all changes.

The plans for the software development in the Sector include the following activities:

- Modification of the database architecture to optimize data interactions;
- The client part is planned to be transferred under the Web platform to increase the flexibility and usability of the system.

***Biomonitoring of air pollution***

In 2017, the summing-up of the activities conducted in 2010-2015 in the framework of the international program "Heavy metal atmospheric deposition in Europe – estimations based on moss analysis" was done (Nickel et al., 2017). In cooperation with the Laboratory of Information Technologies of JINR a cloud system was developed to collect, store and process information on biomonitoring of atmospheric deposition of heavy metals and other toxic elements in the framework of the UN Programme on air of Europe (Uzhinskiy et al., 2017; Kutovskiy et al., 2017; Ужинский, Ососков, Фронтасьева, 2017). In 2017, a review on moss biomonitoring of heavy metal air pollution in Romania was published (Stihi et al., 2017). During the reporting period, a number of papers have been published on the analysis of data of atmospheric deposition of heavy metals and other elements in Albania (Lazo, Steinnes et al., 2017), Serbia (Milićević et al., 2017; Vuković et al., 2017). In cooperation with Adam Mickiewicz University in Poznań we started a NAA study of peat columns from Poland to investigate the retrospective deposition of inorganic atmospheric pollutants. The first results have shown the advantages of using NAA in such studies. On the basis of the analysis of moss-biomonitors an important study of the impact of mining, metallurgical and chemical industries as well as agriculture on the environment of the Tula region was performed. The estimates of atmospheric deposition of toxic elements that accompany these types of environmental contaminants have shown that many of the elements indicate the rising levels of pollution as compared with the previous studies (Gorelova, Frontasyeva, 2017). The results of moss and lichen biomonitoring of air pollution in the Western Cape were reported at the conference in Montenegro (Ntombizikhona Beaulah Ndlovu, M. V. Frontasyeva et al., 2017). In cooperation with the Polish specialists, studies were performed to determine the atmospheric deposition of trace elements on the territory of King George Island in Antarctica (Mroz et al., 2017). In cooperation with the Department of Ecological Chemistry of Baku State University, we conducted an assessment study of air pollution on the Absheron Peninsula in Baku, the capital of Azerbaijan (Gajieva, M.V. Frontasyeva, A.I. Madadzada et.al., 2017).

# SCIENTIFIC HIGHLIGHTS

***Biotechnologies***

In 2017, in cooperation with the microbiologists from the Institute of Microbiology and Biotechnology of the Academy of Sciences of Moldova, work was started on the synthesis of selenium, gold and silver nanoparticles by protein and carbohydrate fractions isolated from cyanobacterial biomass. ). In 2017, the studies of processes of extraction of toxic metals from model solutions and wastewater using microalgae *Spirulina platensis* were continued (Zinicovscaia, Cepoi et al. 2017). In collaboration with the A.N.Frumkin Institute of Physical Chemistry and Electrochemistry of RAS we investigated the processes of accumulation and biosorption of metals (vanadium, chromium, uranium, lanthanum) from mono- and multicomponent systems by bacteria *Pseudomonas putida*. The results obtained showed that the concentrations of metals accumulated by the microbial biomass in the process of bioaccumulation were 15-40 times higher than in the biosorption process (Zinicovscaia, Safoniov et al. 2017). In collaboration with the Institute of Experimental Physics, SAS in Košice a study was conducted on the extraction of heavy metals from model solutions using poplar sawdust (Demcak et al., 2017). In cooperation with the Department of Chemistry of University of the Western Cape, South Africa, we studied the problems of green synthesis of silver-doped titanium dioxide used as an antimicrobial agent. The results were reported at the Symposium on Bacterial Genetics and Ecology in Aberdeen, Scotland (N. Kobese et al., 2017). In cooperation with the M.F.Vladimirskiy Moscow Regional Research and Clinical Institute and National Research Center "Kurchatov Institute", studies were started to evaluate the effect of silver nanoparticles on cognitive functions in mice. The neutron activation analysis was used to determine the silver content in liver, blood and brain samples of mice (Ivlieva, ... Zinicovscaia, Pavlov, Frontasyeva., 2017).

***Environmental assessment***

To continue the work on the assessment of the environmental situation in the basin of the Nile River and its delta, an additional statistical data analysis of the whole amount of the results on soils and sediments was performed (Badawy, E.H.Ghanim et al., 2017) and concentrations of natural and man-made radionuclides in the Nile Valley and its delta were determined (Badawy et al., 2017). In cooperation with the National Research Center in Dokki, Cairo, work was done on modeling the coordination bonds of a number of elements (Na, Mg, Ca, Fe, Ni, and Zn) with organic acids (Okasha et al., 2017). In 2017, NAA studies of coral samples from the Red Sea to assess its pollution by heavy metals and other toxic elements (Abdo et al., 2017) as well as of algae from the coastal aquatic areas of the Mediterranean sea along Alexandria city (Nassar et al., 2017) were carried out in the framework of the Protocol on Cooperation with Cairo University. Within the framework of the pilot project, we performed the analysis of therapeutic muds (peloids) from Cuban SPAs ("Sanus per Aquam", or "Sanitas pro Aqua", which in Latin means "health by means of water" or "health through water").

In collaboration with the A.O.Kovalevsky Institute of Marine Biological Research (Sevastopol) the analysis of the samples of macroalgae-biomonitors (red, green and brown) collected in the coastal zone of the Black Sea for the assessment of the state of the Crimea coastal ecosystem was completed. The study of the seasonal variation of concentrations of 46 elements in phytoplankton of coastal areas of the Black Sea was completed. The obtained results have shown that phytoplankton can be successfully used as a biomonitor of aquatic ecosystems.

In 2017, in cooperation with the Faculty of Biology of Moscow State University the long-term (2014-2016) investigation on the determination of the elemental composition of soil, bottom sediments, terrestrial and aquatic vegetation to assess the transport of pollutants in the strategically important areas of the Black Sea (coastal area of Anapa, Novorossiysk and Tuapse) was completed (P.Nekhoroshkov et al, 2017).

***Analysis of food products***

In cooperation with the specialists of the Moldovan wine industry, geographical origin identification of various wines was performed using a multielement NAA technique (Zinicovscaia, Duliu, Culicov et al., 2017).

***Geology***

In cooperation with the Western Cape University (South Africa) we conducted a NAA study of new samples of coal fly ash from the Matla coal power station in the Mpumalanga province in South Africa, as well as of soil and vegetation. Soil samples obtained from the Institute of Geology and Geophysics of the National Academy of Sciences of Azerbaijan and the National Center for Nuclear Research of Azerbaijan were analyzed as well. For the first time, the analysis of these samples was performed by the neutron activation method. The obtained data are of great practical interest for the Geological Survey of Azerbaijan.

***Analysis of materials of extraterrestrial origin***

In 2017, a multielement NAA of ferrous and carbonaceous meteorites received from the United States and Serbia was performed. For the first time, iridium content was determined in exotic clay samples from the famous Fish Clay collected by Serbian scientists at the coastal cliff Stevns Klint in Denmark. Most researchers believe that the Ir enrichment of this clay resulted from the impact of a chondritic asteroid striking the Earth about 65 millions years ago (P.I. Premović, M.G. Đorđević et al., 2017),

***Medicinal plants***

In 2017, we continued investigations in a new promising line of research – determination of the elemental composition of plants used in medicine. These studies are conducted in cooperation with the specialists from Mongolia and Poland (University of Wrocław and Pedagogical University of Cracow).

***Materials science***

In 2017, in cooperation with the Scientific and Practical Materials Research Center of the National Academy of Sciences of Belarus, a number of investigations of great practical interest were carried out in the framework of the BRFBR-JINR joint grant including studies on crystallization processes and characterization of artificial diamonds, as well as determination of the impurity composition of copper disulphide obtained at high pressures.

**References**

[1] Zeinalov Sh.S., Sedyshev P.V., Shvetsov V.N., Sidorova O.V. Prompt fission neutron investigation in $^{235}U(n_{th},f)$ reaction, EPJ Web of Conferences 146,04022 (2017), ND2016.
[2] V.F. Apalin, Yu. N. Gtitsuk, I.E. Kutikov, V.I. Lebedev, and L.A. Mikaelyan, Nucl. Phys., **55**, 249 (1964).
[3] Geltenbort P., Gonnenwein F., and Oed A., Radiat. Effects, 57, 1986.
[4] Gonnenwein F. ISINN25 Dubna 20-25 May 2017.
[5] T. von Egidy and D. Bucurescu, Phys. Rev. C 72, 044311 (2005).
[6] K.-H. Schmidt., and B. Jurado., Entropy Driven Excitation Energy Sorting in Superfluid Fission Dynamics. Phys. Rev. Lett. 104 212501 (2010)
[7] A. Göök, W. Geerts, F.-J. Hambsch, S. Oberstedt, M. Vidali, Sh. Zeynalov. A position-sensitive twin ionization chamber for fission fragment and prompt neutron correlation experiments, Nucl. Instr. and Meth, *A* 830, 366-374 (2016).
[8] Zeinalov Sh.S., Sedyshev P.V. Sidorova O.V., Shvetsov V.N Numerical simulation and experimental investigation of position sensitive ionization chamber, ISINN25 Dubna 20-25 May 2017.
[9] Zeinalov Sh.S., Sedyshev P.V. Sidorova O.V., Shvetsov V.N. Position sensitive ionization chamber for nuclear fission investigation. Accepted in Journal of Modern Physics: Conference Series; available online at www.creteconf.org/presentations/ShZeinalov_Crete2017.pdf
[10] Strutinsky V.M., *in* Proc. International Congress on Nuclear Physics, Paris, France, 1958, p. 617.
[11] Ignatyuk A.V., Report INDC-233(L), IAEA (Vienna, 1985).
[12] Kadmenskij S.G., Markushev V.P. and Furman W.I, Sov. J. Nucl. Phys. **37,** 165 (1983).
[13] Mingrone F., Altstadt S., Andrzejewski J.,et al., High precision measurement of the radiative capture cross section of 238U at the n_TOF CERN facility, EPJ Web of Conferences 146, 11028, Phys. Rev., C 95, 034604
[14] Balibrea-Correa J., E Mendoza E., D Cano-Ott D., et al., Measurement of the neutron capture cross section of the fissile isotope 235U with the CERN n_TOF total absorption calorimeter and a fission tagging based on micromegas detectors, EPJ Web of Conferences
[15] Mastromarco M., Barbagallo M., Vermeulen M.J.,et al., The 236U neutron capture cross-section measured at the n_TOF CERN facility, EPJ Web of Conferences 146, 11054
[16] Stamatopoulos A., Tsinganis A., Colonna N., et al., Measurement of the 240Pu (n, f) cross-section at the CERN n_TOF facility: First results from experimental area II (EAR-2), EPJ Web of Conferences 146, 04030
[17] Mendoza E., Cano-Ott D., Altstad S. et al., Measurement of the 241Am neutron capture cross section at the n_TOF facility at CERN, EPJ Web of Conferences 146, 11022
[18] Barbagallo M., Colonna N., Aberle O., et al., $^{7}Be$ (n, α) and $^{7}Be$ (n, p) cross-section measurement for the cosmological lithium problem at the n_TOF facility at CERN, EPJ Web of Conferences 146, 01012
[19] Wright T., Guerrerro C., Billowes J., et al. (The n_TOF Collaboration), The $^{33}S(n,\alpha)^{30}Si$ cross section measurement at n_TOF-EAR2 (CERN): From 0.01 eV to the resonance region, Phys. Rev. C **96**, 064601
[20] B. A. Benetskii, I. M. Frank. Angular correlation between gamma rays and 14-mev neutrons scattered inelastically by Carbon // JETP. —1963. — Vol. 17. — P. 309.)
[21] Bazhazhina N.V., Mareev Y.D., Pikelner L.B., Sedyshev P.V., Shvetsov V.N., Analysis of Element and Isotope Composition of Samples by Neutron Spectroscopy at the IREN Facility.Physics of Particles and Nuclei Letters, Volume 12, No. 4, 2015, pp. 578–583